

Recent advances in the rational design of single-atom catalysts for electrochemical CO₂ reduction

Huoliang Gu, Jing Wu, and Liming Zhang (✉)

Department of Chemistry and Shanghai Key Laboratory of Molecular Catalysis and Innovative Materials, Fudan University, Shanghai 200438, China

© Tsinghua University Press 2022

Received: 19 January 2022 / Revised: 21 February 2022 / Accepted: 22 February 2022

ABSTRACT

Electrochemical CO₂ reduction (CO₂R) represents a sustainable way to store intermittent renewable energies and produce carbon-neutral fuels, yet the energy efficiency remains a huge bottleneck owing to its sluggish kinetics and complex reaction pathways. Highly active, selective, and robust electrocatalysts are strongly demanded to accelerate CO₂ conversion and deploy this technology to practical applications. In this review, we focus on single-atom catalysts (SACs), a unique category of electrocatalysts with atomically dispersed metal active sites, which have shown distinctive performances in CO₂R and offer an ideal platform for in-depth mechanistic studies at the atomic level. Despite various SACs with attractive CO₂R performances have been reported, the relationship between electronic/geometric structure of SACs and the corresponding electrocatalytic performance still needs to be discussed with caution. Here we take a broad overview on the recent progress in understanding the structure–function correlation of SACs in CO₂R, with the purpose of providing deep insights and guiding the future rational design of SACs. First, we provide the fundamental understandings of CO₂R on SACs, following different reaction pathways. Then, we describe the progresses in the development of well-defined SACs and the mechanistic studies on the influences from particular structural parameters, such as first-shell and second-sphere coordination, conductive supports and interface with a secondary catalyst. Finally, some perspectives are highlighted on the path towards efficient CO₂R on SACs.

KEYWORDS

single-atom catalysts, electrochemical CO₂ reduction, structure–function correlation, rational design

1 Introduction

In the past few centuries, fossil fuels have played an irreplaceable role in the rapid development of human society. However, the over-reliance on fossil fuels led to an excessive emission of CO₂, which consequently caused the greenhouse effect and broke the natural carbon cycle [1– 3]. Given that, the call for carbon neutralization to mitigate the emission of CO₂ has been placed on the agenda. Electrochemical CO₂ reduction (CO₂R) to value-added fuels and chemicals presents a feasible pathway for renewable energy storage and could help mitigate the ever-increasing CO₂ emissions [4– 6]. When integrated with sustainable energy sources, such as solar and wind, electrochemical CO₂R can effectively store these intermittent renewable energies in stable chemicals and fuels, and help balance the power grid [7– 10]. However, distinguished with proton reduction, CO₂R exhibits multiple reaction pathways typically with rather sluggish kinetics [11– 13]. Despite of tremendous efforts ever since the pioneering work by Hori et al. [14], to date, the main challenge for CO₂R remains the design of highly active, selective, and stable electrocatalysts [15].

Over the past decades, a broad class of electrocatalysts, such as metals, metal oxides, transition-metal chalcogenides/phosphides, molecular complexes, etc., have been developed to improve CO₂R performance [16– 21]. Single-atom catalysts (SACs), defined as a category of catalysts where metal atoms were single-dispersed on a

support without any appreciable interactions, have emerged as potential candidate catalysts because of their unique structures and outstanding performances [22]. As a new type of advanced materials, SACs feature maximized metal utilization, lower-coordinated metal centers, and tunable structures, as well as high activity and selectivity for catalytic reactions [23– 26]. More importantly, the active sites of SACs are all well-defined and atomically isolated on the support, resulting in a uniform chemical environment surrounding, and are thus predicted to be an ideal model system to bridge the homogeneous and heterogeneous catalysis [27, 28]. In 2011, Qiao et al. first reported a single-atom platinum catalyst stabilized on iron oxide nanocrystallites (Pt₁/FeO_x), which displayed an extremely high atomic utilization efficiency, excellent stability, and activity [29]. With the rapid development of advanced *in/ex-situ* characterization techniques, such as X-ray absorption spectroscopy (XAS) and high-angle annular dark-field scanning transmission electron microscopy (HAADF-STEM), etc., the accurate structural characterization of isolated metal centers brings in more understanding and design principles for SACs [30– 32]. Soon afterwards, a variety of SACs including noble metals (Au, Ag, Pt, Ru, Ir, etc.) [33– 36], non-noble metals (Fe, Co, Ni, Cu, Mn, etc.) [37– 41], and bimetals (Pt-Au, Ir-Mo, Pt-Ru, Ni-Ru, etc.) [42– 46] have been reported, exhibiting superior activity and/or selectivity compared to corresponding nanoparticles and clusters in the field of

Address correspondence to zhanglm@fudan.edu.cn



thermocatalysis. Given the great breakthrough achieved by SACs in thermocatalysis, the concept of SACs is thereupon introduced to electrocatalysis, and has been extensively studied for electrochemical hydrogen evolution reaction (HER), oxygen reduction reaction (ORR), oxygen evolution reaction (OER), CO₂R, and recently for nitrogen reduction reaction (NRR) [47–57].

Compared with other heterogeneous catalysts, the unique advantages of SACs qualify them as marvelous electrocatalysts for CO₂R with high performance, providing an ideal model system for understanding the structure–function correlation because of the uniform chemical environment surrounding the active sites [58–60]. Despite that numerous SACs for CO₂R with impressive results are reported, the correlation between electronic states/geometric structure of the active sites and electrocatalytic performance still needs to be discussed with caution. In this review, we aim to provide an overview on recent progresses in the applications of SACs for electrochemical CO₂R, focusing on the impact of electronic states and geometric structures on the electrocatalytic activity and selectivity. Firstly, we will give a brief overview of background and fundamental understanding of the electrochemical CO₂R on SACs. Following, examples of recent advances in the development of well-defined SACs and the structure–function correlation of CO₂R are described. We will review how the structures of SACs, such as coordination environment, conductive support, and interface with a secondary catalyst, influence the activity and selectivity. Finally, we will briefly discuss the future directions, challenges, and opportunities in this fascinating research area.

2 Fundamental understanding of electrochemical CO₂R on SACs

Compared with other electrochemical conversion reactions of small energy-related molecules, such as HER, ORR, OER, and NRR, CO₂R suffers from a much more complex kinetics and multiple reaction pathways associated with 2–18 electrons transfer, leading to a broad range of value-added carbon fuels, e.g., CO and formate, both of which are generated from 2e⁻ pathways, and a series of higher order products from multiple >2e⁻ pathways, such as methane, ethylene, ethanol, and n-propanol [11, 61–65]. For a breakthrough, it is crucial to regulate and improve the selectivity of CO₂R for a specific reduction product and meanwhile to suppress the competing hydrogen evolution from proton reduction [66–68]. In this regard, fundamental understanding of electrochemical CO₂R is strongly demanded for the rational design of highly active, selective, and stable catalysts.

The reaction mechanism of CO₂R has been intensively studied during the past few decades through either *in-situ* spectroscopic measurements or computational simulations based on density functional theory (DFT) [5, 69–72]. While there remains a distinct lack of consensus in this field about some of the reaction steps, CO₂⁺ species, which has a lower energy barrier to accept another electron due to the molecular symmetry broken, is generally believed to form through the activation of CO₂ molecules, and initialize CO₂R [69, 73, 74]. Afterwards, the adsorbed intermediates will undergo several electron/proton transfer steps till final products are produced. Table 1 and Fig. 1 demonstrate multiple reaction pathways of CO₂R with their corresponding thermodynamic potentials [5, 11, 65, 75]. For the sake of discussion, these produced value-added chemicals would be grouped to 2e⁻ products and >2e⁻ products. Following, we will discuss the typical CO₂R reaction pathways on SACs.

Table 1 Electrochemical reactions with equilibrium potentials in aqueous solutions (E vs. standard hydrogen electrode (SHE) pH = 7)

Reaction	E vs. SHE (V)
CO ₂ (g) + * + e ⁻ = *CO ₂ ⁺	-1.85
CO ₂ (g) + 2H ⁺ + 2e ⁻ = HCOOH(l)	-0.61
CO ₂ (g) + 2H ⁺ + 2e ⁻ = CO(g) + H ₂ O(l)	-0.52
CO ₂ (g) + 4H ⁺ + 4e ⁻ = CH ₂ O(l) + H ₂ O(l)	-0.48
CO ₂ (g) + 6H ⁺ + 6e ⁻ = CH ₃ OH(l) + H ₂ O(l)	-0.38
CO ₂ (g) + 8H ⁺ + 8e ⁻ = CH ₄ (g) + 2H ₂ O(l)	-0.24
2CO ₂ (g) + 12H ⁺ + 12e ⁻ = C ₂ H ₄ (g) + 4H ₂ O(l)	-0.35
2CO ₂ (g) + 12H ⁺ + 12e ⁻ = C ₂ H ₆ (g) + 3H ₂ O(l)	-0.33
2CO ₂ (g) + 14H ⁺ + 14e ⁻ = C ₂ H ₆ (g) + 4H ₂ O(l)	-0.27
3CO ₂ (g) + 18H ⁺ + 18e ⁻ = C ₃ H ₇ OH(l) + 5H ₂ O(l)	-0.31

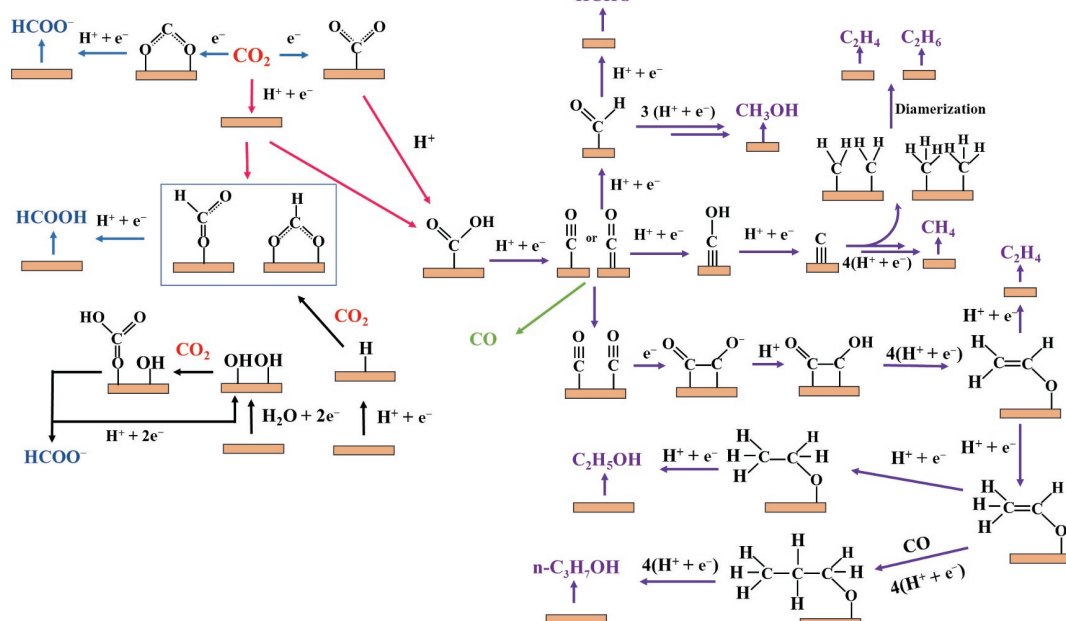


Figure 1 Possible reaction pathways of electrochemical CO₂ conversion, leading to a wide range of products.

2.1 Electrochemical converting CO₂ to 2e⁻ products on SACs

2e⁻ products include CO and formate, two simplest fuels from CO₂R. In particular, CO is the most commonly seen product from CO₂R on SACs. Despite much efforts have been devoted to identifying the reaction pathways and interpreting the activity trends towards CO₂-to-CO conversion, the reaction mechanism is still disputed. Nevertheless, the pathway of CO₂R to CO via a carboxyl (*COOH) intermediate is widely accepted, either through a proton coupled electron transfer (PCET) process or electron transfer followed by a proton transfer process [76–79]. The *COOH intermediate will then convert to *CO via another proton-electron transfer. Finally, weakly bonded *CO desorbs from surface to generate CO product. Along the reaction pathway, the catalytic active sites will be poisoned by either *CO or other intermediates adsorbed on SACs too strongly, and HER will dominate the reaction [80–82]. In this regard, tuning appropriate adsorption energy of intermediate with

metallic center is of significant importance.

Dating back to 1970s, metal complex molecular catalysts with isolated metal centers including Co, Ni, Fe, Mn, etc., have been studied for CO₂R [83–86]. The metal atoms in SACs act as the active sites for CO₂ conversion. To get a brief overview on the performance of SACs with different metal active sites, we summarized some typical SACs, categorized by the metal centers in Table 2. It is apparent that the activity for CO production is primarily depended on the metal sites. Typically, Ni, Co, and Fe were proved to be the most profitable SACs to produce CO, exhibiting marvelous performances with low costs. Lin et al. synthesized covalent organic frameworks comprising CoN₄ active sites and acquired a dramatically high faradaic efficiency (FE) of 90% with a turnover number up to 290,000 h⁻¹ for CO under a low overpotential [87]. Chen et al. prepared a Ni-SAC anchored on ordered mesoporous carbon, which can reach an industrial-level current density of 366 mA·cm⁻² with a FE of CO > 95% in a flow cell [88]. Ni et al. built FeN₄ sites anchored on defect-rich

Table 2 Catalytic performances of SACs for CO₂R

Central metal	Electrolyte	Potential (V _{RHE})	Current density (mA·cm ⁻²)	Product	FE (%)	References
Fe	0.1 M KHCO ₃	-0.95	-33	CO	~ 90	[89]
Fe	0.1 M KHCO ₃	-0.6	~ -1	CO	93	[90]
Fe	0.5 M KHCO ₃	-0.48	-20	CO	~ 96	[124]
Fe	0.1 M NaHCO ₃	-0.6	-4.5	CO	91	[112]
Fe	0.5 M KHCO ₃	-0.43	~ -5	CO	~ 97	[141]
Co	0.5 M KHCO ₃	-0.67	-3.3	CO	91	[87]
Co	0.5 M KHCO ₃	-0.61	-18.7	CO	~ 90	[121]
Co	0.5 M KHCO ₃	-0.78	-32.7	CO	94	[125]
Co	0.1 M NaH ₂ PO ₄	-0.73	~ -2	CO	~ 90	[131]
Co	0.2 M NaHCO ₃	-0.79	-10.2	CO	99.3	[132]
Co	0.1 M KHCO ₃	-0.6	-1.1	CO	83	[137]
Co	0.1 M KHCO ₃	-0.63	~ -10	CO	92	[142]
Co	0.1 M KHCO ₃	-0.9	~ -9	CO	96	[146]
Ni	1 M KOH	-0.8	-51	CO	90	[88]
Ni	0.5 M KHCO ₃	-0.81	-28.6	CO	99	[120]
Ni	0.5 M KHCO ₃	-0.72	-22	CO	98	[128]
Ni	0.5 M KHCO ₃	-0.8	-48	CO	94	[126]
Ni	0.5 M KHCO ₃	-0.93	-31.4	CO	97.5	[127]
Ag	0.5 M KHCO ₃	-0.85	-2.5	CO	95.7	[113]
Pd	0.5 M KHCO ₃	-0.8	-8	CO	63	[155]
Zn	1 M KHCO ₃	-1.8 V _{SCE}	-39.9	CH ₄	84	[105]
Mn	0.5 M KHCO ₃	-0.60	-10	CO	97	[133]
Mo	EmimBF ₄ :H ₂ O = 4:96	-1.4	-193	HCOO ⁻	29	[94]
Sn	0.25 M KHCO ₃	-1.6 V _{SCE}	-11.7	HCOO ⁻	75.1	[96]
Sb	0.5 M KHCO ₃	-0.8	~ -2.5	HCOO ⁻	94	[97]
In	0.5 M KHCO ₃	-0.65	-8.9	HCOO ⁻	96	[95]
Cu	0.5 M KHCO ₃	-1.44	-31	CH ₄	78	[104]
Cu	0.1 M KHCO ₃	-0.9	-93	MeOH	44	[106]
Cu	0.1 M KHCO ₃	-1.4	~ -27.5	C ₂ H ₄	24.8	[107]
Cu	0.1 M KHCO ₃	-1.6	~ -38.3	CH ₄	38.6	[107]
Cu	0.1 M KHCO ₃	-0.36	~ -5	Acetone	36.7	[108]
Cu	0.5 M KHCO ₃	-0.98	-49	CH ₄	27	[138]
Cu	0.5 M KHCO ₃	-0.98	-49	C ₂ H ₄	17	[138]

porous carbon, which shows a remarkable performance towards CO production, achieving a partial current density of $33 \text{ mA}\cdot\text{cm}^{-2}$ with a FE of 90% in 0.1 M KHCO₃ [89]. Similarly, the current density of single-Fe-doped graphitic carbon nitride (FeN₄/C) at -0.8 V versus reversible hydrogen electrode (RHE, V_{RHE}) is 35 and 17 folds higher than those of N/C and Fe/C, respectively [90].

Apart from CO, the production of formate, another $2e^-$ product, is also pursued on SACs due to its broad interest in energy conversion and storage [91]. Formate is expected to originate from a distinguished reaction pathway, as shown in Fig. 1, HCOO* intermediate binds to the catalyst surface primarily through oxygen atom(s) instead of carbon atom. As experiments and DFT calculations suggest, this intermediate may yield from two different ways: (1) CO₂* firstly binds to the catalyst surface, then suffers from a PCET process to produce HCOO*; (2) CO₂ directly inserts into a metal –hydrogen or metal –hydroxy bond to produce HCOO* [11, 92]. From the reported studies, p-block metal atoms such as In, Sn, Bi, and Pd were generally considered as active centers to produce formate [93]. Huang et al. designed and fabricated Mo-SACs by embedding isolated Mo atoms into N-doped graphene, and observed the formate production rate was greatly boosted, attaining a high yield of 747 mmol·g_{catal}⁻¹·h⁻¹ (Fig. 2(a)) [94]. Beyond transition metals, main group metals (In, Sn, Sb, Bi, etc.) have attracted marvelous attention recently due to their great potentials in converting CO₂ to formate, owing to their moderate adsorption energies for

HCOO* intermediates [95]. For instance, Sn-SACs displayed an onset overpotential down to 60 mV for formate production and a large turn-over frequency (TOF) up to 11,930 h⁻¹, with a 200-h stable running [96]. Synchrotron-radiation X-ray absorption near-edge structure (XANES) indicated that positive charges on Sn^{δ+} can stabilize the adsorption of CO₂* and HCOO*, enabling the simultaneous CO₂ activation and CO₂* protonation (Fig. 2(b)). Further, the doped N atoms promoted the desorption of formate (rate-determining step (RDS)) through weakening its bonding strength with Sn (Fig. 2(c)). Detailed electrochemical analysis showed that Sb^{δ+}N₄ moieties exhibited a formate FE of 94% at $-0.8 \text{ V}_{\text{RHE}}$ (Fig. 2(d)) [97]. Soon afterwards, Shang et al. designed a single-atom In^{δ+}N₄ catalysts with a formate FE of 96% at a potential of $-0.65 \text{ V}_{\text{RHE}}$ (Fig. 2(e)) [95]. DFT calculation revealed that the formation free energy of HCOO* was lower than that of COOH* on active sites, resulting in formate be the major product in CO₂R. Moreover, they expanded their strategy to other main group metals like Sn and Sb, which also can achieve a FE of formate over 80%.

2.2 >2e⁻ products generation on SACs

>2e⁻ products can further be grouped to C₁ and C₂₊ chemicals. C₁ products include methane, formaldehyde, and methanol, and C₂₊ products mainly contain ethylene, ethane, ethanol, n-propanol, etc. It is notable that *CO was generally believed to play a deterministic role in the reaction pathways leading to >2e⁻

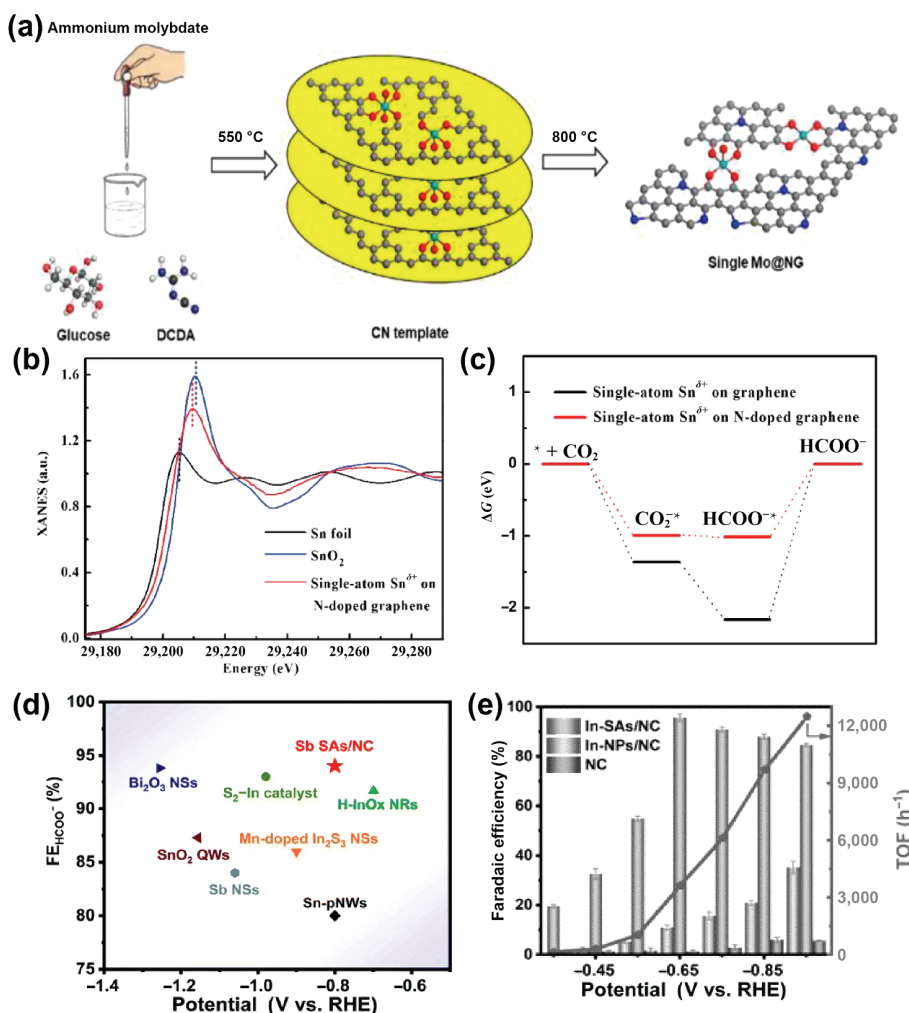


Figure 2 (a) Illustration of preparing Mo-SAC on N-doped graphene. Reproduced with permission from Ref. [94], © Elsevier Ltd. 2019. (b) XANES of Sn foil, SnO₂, and single-atom Sn^{δ+} on N-doped graphene. (c) Calculated free energy diagrams for CO₂R to formate. Reproduced with permission from Ref. [96], © WILEY-VCH Verlag GmbH & Co. KGaA, Weinheim 2019. (d) Formate FEs of Sb-SAC compared with other catalysts. Reproduced with permission from Ref. [97], © The Royal Society of Chemistry 2020. (e) FEs and TOF of formate at different potentials. Reproduced with permission from Ref. [95], © Wiley-VCH GmbH 2020.

products [12, 64, 76, 79]. C_1 products are very likely to undergo the route where $^*\text{CO}$ reacts with a concerted proton–electron (H^+/e^-) from solution to generate intermediate species, such as $^*\text{CHO}$, $^*\text{CH}_2\text{O}$, $^*\text{CH}_3$, and $^*\text{OCH}_3$. Peterson et al. suggested that a most thermodynamically favorable pathway leading to C_1 involves the initial $^*\text{CO}$ hydrogenation to produce adsorbed $^*\text{CHO}$, followed by the addition of proton–electron pair to successively generate $^*\text{CH}_2\text{O}$ (which can be alternatively desorbed as formaldehyde) and then $^*\text{OCH}_3$. Ultimately, $^*\text{OCH}_3$ can be further reduced to methane [98]. Considering that formaldehyde ($^*\text{CH}_2\text{O}$) can only be reduced to methanol other than methane, the oxophilicity of the catalyst surface, as determined by the binding energy of O_{ads} , plays a key role in switching the selectivity between methane and methanol. For example, Kuhl et al. reported that only methanol was detected on the poorly oxophilic Au, whereas only methane was detected on strongly oxophilic Fe [99]. The similar trend can also be observed in C_{ads} , and therefore the modification of the binding energy for C_{ads} and O_{ads} will directly influence the C_1 product distribution. In addition, Nie et al. proposed another new mechanism for methane production based on theoretical analysis which involved the discussion of kinetic barriers [100]. In this study, $^*\text{CO}$ is inferred to turn into $^*\text{COH}$ intermediate, followed by being reduced to an adsorbed carbon atom ($^*\text{C}$), and further reduced successively to $^*\text{CH}$, $^*\text{CH}_2$, $^*\text{CH}_3$, and ultimately CH_4 .

As we can see, the reduction pathway of C_1 product remains

ambiguous, the understanding towards the formation of C_{2+} product is even more challenging. Among various heterogeneous CO_2R catalysts, Cu-based catalysts are the only widely-accepted catalysts capable to reduce CO_2 to C_{2+} chemicals due to its moderate binding energy with key intermediates (i.e., CO^*) [101]. In CO_2R to C_{2+} products, C–C coupling is the most discussed and yet controversial step in the proposed mechanisms. Different pathways have been proposed for C–C bond formation, including 1) direct dimerization of $^*\text{CO}$ (i.e., $^*\text{OCCO}$ formation), 2) $^*\text{CO}$ coupling with another hydrogenated $^*\text{CO}$ such as $^*\text{COH}$ and $^*\text{CHO}$ (i.e., $^*\text{OCCHO}$ or $^*\text{OCCOH}$ formation), 3) dimerization of two hydrogenated $^*\text{CO}$ (i.e., $^*\text{HOCCOH}$ formation), and 4) coupling of C_1 intermediates such as $^*\text{C}$, $^*\text{CH}$, or $^*\text{CH}_2$ to form $^*\text{CC}$, $^*\text{HCH}$, or $^*\text{H}_2\text{CCH}_2$ [78]. It is also worth to mention that the carbon dimerization process can be strongly affected by both the nature of catalysts and external reaction environments, which makes the study of C_{2+} products even more of controversy [102, 103].

With strongly adsorbed CO^* on metal centers, $> 2\text{e}^-$ products are likely to generate on SACs, in particular C_1 , such as methane and methanol. Cai et al. designed SACs with numerous CuN_2O_2 sites which can electrochemically reduce CO_2 to methane with a remarkable FE of 78% at $-1.44 \text{ V}_{\text{RHE}}$ [104]. Han et al. fabricated a microporous N-doped carbon supported Zn-SAC, which favored a multi-electron transferring pathway to produce methane (Fig.

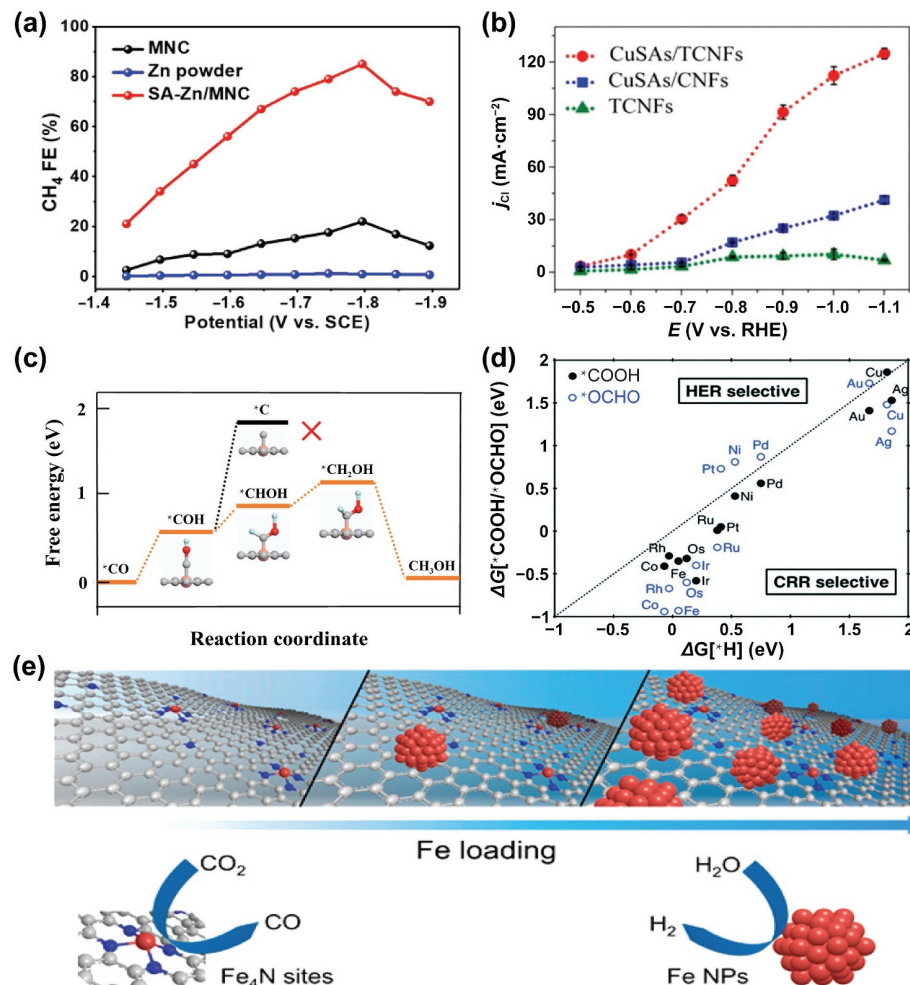


Figure 3 (a) FEs for CO_2 to methane at different applied potentials. Reproduced with permission from Ref. [105], © American Chemical Society 2020. (b) Partial current density of C_1 products for three catalysts. (c) Free energy diagram of $^*\text{CO}$ conversion to methanol on CuN_4 structure. Orange, gray, dark blue, red, and light blue spheres stand for Cu, C, N, O, and H atoms, respectively. Reproduced with permission from Ref. [106], © American Chemical Society 2019. (d) Free energy change of the first protonation step in CO_2R and HER on various SACs. Metals below the dotted line are CO_2R selective. Reproduced with permission from Ref. [111], © The Royal Society of Chemistry 2017. (e) Illustration of structure-selectivity relationship in Fe-N-C materials. Reproduced with permission from Ref. [112], © American Chemical Society 2017.

3(a)) [105]. This catalyst exhibited a maximum FE of 85% with an excellent stability over 35 h. DFT revealed that O rather than C atom in $^*\text{OCHO}$ prefers to bind with Zn, suppressing the generation of CO and enhancing methane production. Yang et al. developed a single atomic Cu-decorated carbon nanofiber catalyst for CO_2R . The uniformly isolated CuN_4 active centers exhibited a 44% FE towards methanol and a 50-h long term durability (Fig. 3(b)) [106]. DFT results indicated that the desorption step of $^*\text{CO}$ is slightly endergonic over CuN_4 (0.12 eV) in relative to the typical SACs, suggesting $^*\text{CO}$ is prone to be further reduced to COH^* instead of being released as CO. Free energy diagram showed that the reduction of CO^* to methanol on CuN_4 has a moderate free energy barrier (0.86 eV), whereas the barrier of $^*\text{COH}$ to $^*\text{C}$ (1.88 eV) was higher than any steps along methanol formation pathway (Fig. 3(c)). Therefore, methanol instead of methane was the ultimate product on CuN_4 catalysts.

Although Cu is distinctive in its ability to reduce CO_2 to C_{2+} products with substantial yields, C_{2+} fuels production on Cu-SACs is rarely reported because the essential C–C dimerization pathway is substantially blocked on isolated Cu sites [104]. To date, only a few examples have shown the capability of Cu-SACs for C_{2+} production. For example, Guan et al. demonstrated a Cu-SAC dispersed on nitrogen-doped carbon that can produce ethylene, with a partial current density of 6.84 mA·cm⁻² and FE of 24.8% at $-1.4 \text{ V}_{\text{RHE}}$ [107]. Zhao et al. designed a Cu-SAC anchored on N-doped porous carbon as catalysts that can produce ethanol, acetate, and acetone [108]. In particular, the production rate of acetone can reach 336.1 $\mu\text{g}\cdot\text{h}^{-1}$ with a record FE of 36.7%. Overall, CO_2R to value-added products beyond CO and formate on SACs remains a grand challenge. Increasing the binding energy between key intermediate CO^* and metal centers is a possible way to suppress the release of CO and enhance the reaction pathway towards further reduced products. Single-site Cu can undergo reconstruction to nanoclusters at suitable potentials during electrolysis, which could help to improve the selectivities of C_{2+} products in CO_2R [109, 110]. However, it is worth to note that too strong binding energy may lead to metal center poison, thereby leading to CO_2R deactivation [11]. In addition, reducing CO_2 into more energy-dense liquid C_{2+} products holds great promise. To overcome the geometrical limitation of C–C coupling on isolated metal centers, atomic dual-metal sites may open up more opportunities for CO_2R into C_{2+} fuels, where more than one active centers are demanded to create synergistic interactions.

2.3 Suppression of HER pathway on some particular SACs

Another significant advantage of SACs is its capability to suppress the major competing hydrogen evolution during CO_2R . Theoretical calculation compared the first protonation step of HER and CO_2R , which showed that the formation of $^*\text{COOH}$ and/or $^*\text{OCHO}$ was more preferable than $^*\text{H}$ on most SACs (Fig. 3(d)), suggesting that SACs are benefiting to suppress the major competing HER, and promote CO_2R [111]. For example, Huan et al. experimentally evaluated the product distribution of CO_2R on catalysts with various ratios of isolated Fe atomic sites and Fe nanoclusters, and demonstrated that the product selectivity strongly depended on the fraction ratio of isolated Fe sites (Fig. 3(e)) [112]. A FE of CO over 90% was achieved at $-0.6 \text{ V}_{\text{RHE}}$ with a higher particular content of Fe-SAC. Zhang et al. reported Ag single atom on MnO_2 which showed a greater performance than Ag nanoparticles on MnO_2 , achieving 95.7% FE at $-0.85 \text{ V}_{\text{RHE}}$. The DFT results showed that HER could occur on Ag/ MnO_2 only at high overpotentials, and HER can be well suppressed within a

low overpotential range [113]. Bagger et al. further explained the distinguished product generation on isolated metal SACs [114]. Typically, HER follows either Volmer–Tafel or Volmer–Heyrovsky mechanism. DFT calculations indicated that HER on different bulk metals usually follow Volmer–Tafel mechanism since the Tafel reaction, two adsorbed H^* undergo a coupling step to form $\text{H}_2(\text{g})$, is much more favorable than the Heyrovsky reaction. However, the Tafel mechanism requires at least two adjacent active sites for H^* adsorption, which will unlikely to happen on SACs. Towards this end, the Volmer–Heyrovsky mechanism with a much higher activation barrier proceeds as the dominant pathway on SACs, and thus HER is remarkably suppressed in relative to their bulk metal counterparts. It is also worth to note that not all SACs have the capability to suppress HER, instead, some particular SACs demonstrate remarkable performances for proton reduction [115–118]. These different catalytic behaviors of SACs for HER and CO_2R may come from the distinguished electronic structures of metal centers, ligands, and external reaction environments (pH value, local CO_2 concentration, etc.). Beyond that, the mass transfer limitation of CO_2R is significant at higher overpotentials because of the poor solubility of CO_2 and its equilibria in aqueous electrolyte, leading to a grand challenge to achieve high CO_2 conversion rate [64]. To accurately investigate the CO_2R kinetics, the studies should focus on the low and/or moderate overpotential region, where the influences from CO_2 supply are minor and thus the comparison of the catalytic performance is meaningful. To address the mass transfer limitation of CO_2 , various strategies have been proposed, such as using a gas-fed reactor, which will be discussed later in this review.

3 Structure–function correlations of SACs in electrochemical CO_2R

As discussed in the fundamentals of CO_2R on SACs, the electronic structure of the metal center strongly affects the formation and adsorption/desorption of key intermediates, and plays a deterministic role in the product selectivity. Regulating the local environments of metal sites is regarded as an efficient way to optimize the electronic structures of metal centers, and therefore, is critically important to improve the performance towards CO_2R . Beyond that, SACs typically exhibit a high efficiency in producing $2e^-$ products, in particular CO, rather than $> 2e^-$ products. Developing a synergistic and/or a tandem catalytical system will contribute to enhance the yields towards more value-added and deeply reduced chemicals. In this section, we will highlight structure–function correlation of SACs in CO_2R from the following three aspects: the coordination environment, the conductive support effect, and the synergistic/tandem catalytic system.

3.1 Coordination environment

The coordination environments can stabilize metal atoms; thus, it is of equal importance to the metal centers, and in some situations, it is even a dominant factor to determine the activity, selectivity, and stability of SACs. Deciphering how coordination environment affects the CO_2R performance is a cornerstone of designing highly efficient SACs. Typically, the influences include two scenarios: the first-shell heteroatom coordination (direct coordination) and the second-sphere interaction (indirect coordination). The first-shell heteroatom coordination, including coordination atoms, numbers, axial chemical environments, etc., can directly influence the electronic structure and/or oxidation state of the metal center. Although the second-sphere environment, such as substituents on

ligands, has no direct interaction with the metal center, it is also capable to regulate the CO₂R performance in some extent. Following, we will discuss the coordination environments impacts in these two scenarios respectively.

3.1.1 The first-shell heteroatom coordination

In the past decade, SACs supported on heteroatom doped carbon materials (denoted as M-X-C catalysts, X = N, O, S, P, etc.) are emerging as a large category of SACs for CO₂R because of their outstanding electrochemical activity, selectivity, and durability. Among these, N is the most extensively studied heteroatom to coordinate with the metal center [119]. Dating back to 1974, Meshitsuka et al. first studied the polarization curves of Co- and Ni-phthalocyanines with MN₄ centers attached on graphite electrodes for electrochemical CO₂R [83]. MN₄ is hitherto regarded as a highly efficient active site. For example, NiN₄ exhibited a high FE of CO over 90% across the full potential window of CO₂R, together with a maximum FE of 99% and a partial current density of 28.6 mA·cm⁻² (Fig. 4(a)) [120]. CoN₄ and FeN₄ showed similar results as NiN₄ [121, 122]. Notably, the types of coordinated N atoms have a strong impact on the valence state of central metal as well as electrochemical performance. Wang et al. discovered that the energetically favorable pyrrolic-type NiN₄ moiety displayed highly-selective CO₂R over the competing HER through a constant-potential first-principle and microkinetic model (Figs. 4(b) and 4(c)) [123]. In experiment, Gu et al. synthesized atomically dispersed Fe³⁺-N-C sites by pyrolysis of Fe-doped Zn 2-methylimidazolate framework (ZIF-8) and prepared a reference sample (Fe³⁺-N-C) through pyrolysis of a Fe-phenanthroline complex. X-ray photoelectron spectroscopy (XPS) confirmed that the central Fe³⁺ in Fe³⁺-N-C coordinated with

pyrrolic N whereas the Fe²⁺ atom coordinated with pyridinic N in Fe²⁺-N-C. Pyrrolic N coordinated and atomically dispersed Fe³⁺ ions maintained their initial oxidation state under CO₂R electrocatalysis and consequently exhibited an outstanding activity and stability, producing CO at an overpotential as low as 80 mV and achieving an 80% FE across a wide potential window. In stark contrast, pyridinic N coordinated Fe²⁺ ions in Fe²⁺-N-C exhibited a poor activity under the identical condition [124]. The significance of coordination N types was also proved by Cu-SACs on N-doped carbon. Cu-N-C having a higher pyrrolic N and lower pyridinic N contents is confirmed to display a superior performance in converting CO₂ to acetone. DFT simulations authenticated that the Cu-pyrrolic-N₄ active site has advantages in stabilizing the reaction intermediates *COOH involved in acetone production, favoring the C–C coupling process (Fig. 4(d)) [108].

The coordination number between metal center and N is another nonnegligible parameter. Heat treatment is an effective way to regulate the metal–N coordination number. Wang et al. designed Co-SACs with a controlled Co–N coordination number from 4 to 2 by tuning the pyrolysis temperature (Fig. 4(e)) [125]. They found that the CoN₂ site unexpectedly exhibited a much higher catalytic activity and selectivity as compared to CoN₃ and CoN₄, because the decreased coordination numbers of N could result in more unoccupied 3d orbitals of Co atoms, which can promote the adsorption of CO₂[–] and accelerate the reaction. The distinguished performance of CoN₂ was also supported by its lowest charge transfer resistance among three catalysts. Additionally, the active CoN₂ sites showed a long-term stability at a time scale of 60 h. Rong et al. proposed that the presence of vacancy defect in NiN_x plays a key role in

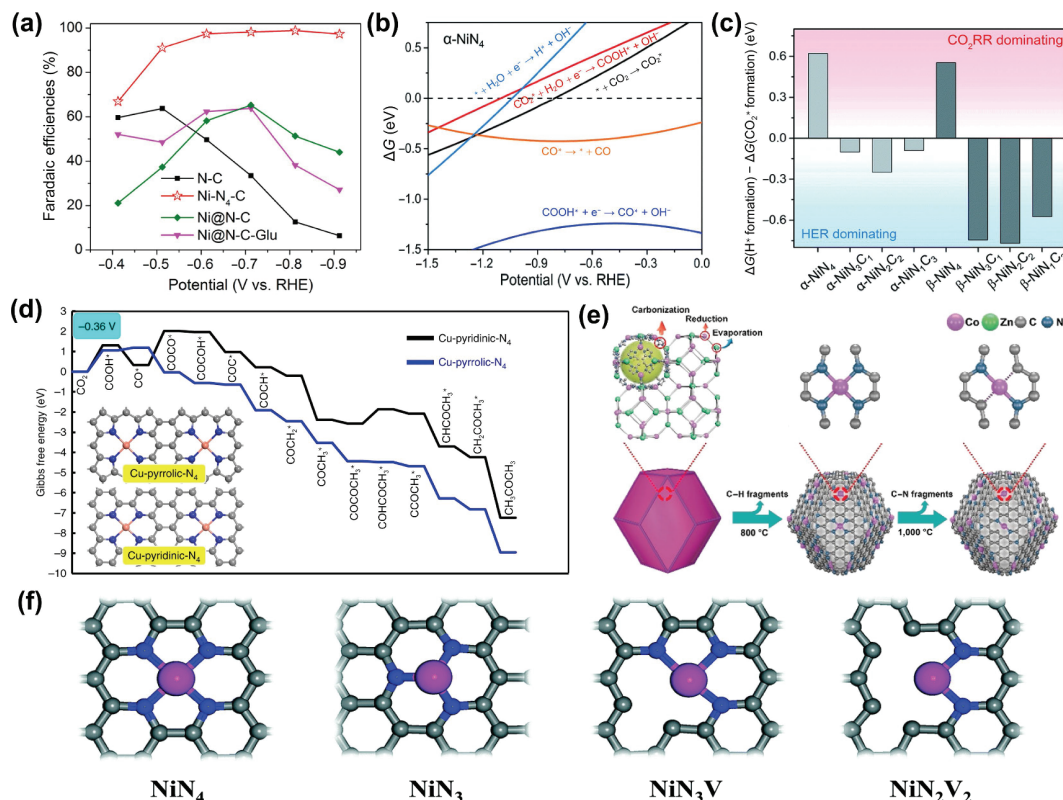


Figure 4 (a) FEs of CO at different potentials for catalysts. Reproduced with permission from Ref. [120], © American Chemical Society 2017. (b) Free energy changes along different reaction steps on α -NiN₄. (c) Difference in free energy between H⁺ formation and CO₂^{*} formation at $U = -0.60$ V. A more positive value means higher CO₂R selectivity, and a more negative value means higher HER selectivity. Reproduced with permission from Ref. [123] © The Royal Society of Chemistry 2021. (d) Free energy diagrams calculated at a potential of -0.36 V for CO₂R to acetone on Cu-pyridinic-N₄ and Cu-pyrrolic-N₄ sites of Cu-SAC/NPC (the computational models were included in the figure). Reproduced with permission from Ref. [108], © Zhao, K. et al. 2020. (e) The formation process of CoN₄ and CoN₂. Reproduced with permission from Ref. [125], © Wiley-VCH Verlag GmbH & Co. KGaA, Weinheim 2018. (f) Optimized atomic structures of different Ni-N structures. Reproduced with permission from Ref. [127], © The Royal Society of Chemistry 2018.

boosting CO₂R by lowering the energy barrier for COOH* formation and CO desorption [126]. Yan et al. obtained a similar conclusion deduced from SACs with NiN₄ and coordinatively unsaturated sites NiN₃, NiN₃V, and NiN₂V₂ (V stands for coordination vacancy) (Fig. 4(f)) [127]. DFT calculation suggested that G_{COOH} on unsaturated NiN₃, NiN₃V, and NiN₂V₂ are significantly lower than that on NiN₄, suggesting those coordinatively unsaturated Ni-N sites would greatly contribute to the high CO₂R activity.

Furthermore, SACs supported on dual-heteroatoms (N, O, S, P, etc.) doped carbon materials are observed to promote CO₂R. S, N-doped Ni-SAC showed a lower onset potential compared to the pure N-doped catalyst [128]. The Ni atoms were coordinated to S and pyridinic N, which exhibits a weaker electronegativity than the pyrrolic N in Ni(II)Pc, resulting in Ni(I) center with a d⁰ electronic configuration. Consequently, the catalyst achieved a specific current density of 350 A·g_{catalyst}⁻¹ and a TOF of 14,800 h⁻¹ at an overpotential of 0.61 V with a 97% FE of CO and a 100-h catalytic stability. Kim et al. investigated Ni sites with well-defined coordination of tetraphenylporphyrin (N₄-TPP) and 21-oxatetraphenylporphyrin (N₃O-TPP) (Figs. 5(a) and 5(b)) [129]. Spectroscopy and computational studies revealed that the broken ligand-field symmetry is a key factor for CO₂R activation, which subordinates an increase in Ni redox potential towards Ni(I). However, there are other opposite views to what were observed above. Hossain et al. theoretically applied grand canonical potential kinetics formulation of quantum mechanics to predict the reaction mechanism and rates for CO₂R over Ni-SACs

including NiN₂C₂, NiN₃C₁, and NiN₄ sites [130]. NiN₄ exhibited the best performance among the three catalysts, reaching 40 mA·cm⁻² with a FE of 100% at $U = -1.05$ V. Moreover, their study revealed that, compared to NiN₄, NiN_{4-x}C_x was capable to facilitate CO₂R at a lower overpotential (Fig. 5(c)).

Adding an axial ligand to form a five-coordinated structure is another route to tune the activity of SACs. The axial coordination environment of metal centers in SACs can be regulated by the axial interactions with supports. It was observed that a five-coordinated cobalt phthalocyanine (CoPc)-poly-4-vinylpyridine (P₄VP) exhibited a superior performance than primitive CoPc in 0.1 M NaH₂PO₄ buffer solution at pH 4.7. The axial coordination raises the energy of Co d_{z²} orbital, as a result, the central Co(I) becomes a stronger nucleophile, binding and activating the Lewis acidic carbon of CO₂ more easily (Fig. 5(d)) [131]. Pan et al. developed an atomically dispersed CoN₅ site anchored on polymer-derived hollow N-doped porous carbon spheres (CoN₅/HNPCSS). The CoN₅/HNPCSS catalyst exhibited a high FE of CO (99.4%) at -0.79 V_{RHE} [132]. The preeminent results can be attributed to the low free energy of *COOH formation and moderate binding energy of CO on CoN₅ sites (Fig. 5(e)). Apart from those widely-used axially coordinated N and O atoms, halogen atoms can boost CO₂R as well. Zhang et al. depicted a single Mn-SACs ((Cl, N)-Mn/G) which was coordinated with four equatorial N atoms and an axial Cl atom [133]. The (Cl, N)-Mn/G catalyst displayed a high TOF of 38,347 h⁻¹ at -0.6 V_{RHE}, which was fifty-fold higher than that on N-Mn/G. Computational simulation suggested that Cl coordination and distorted Mn center resulted in a strong

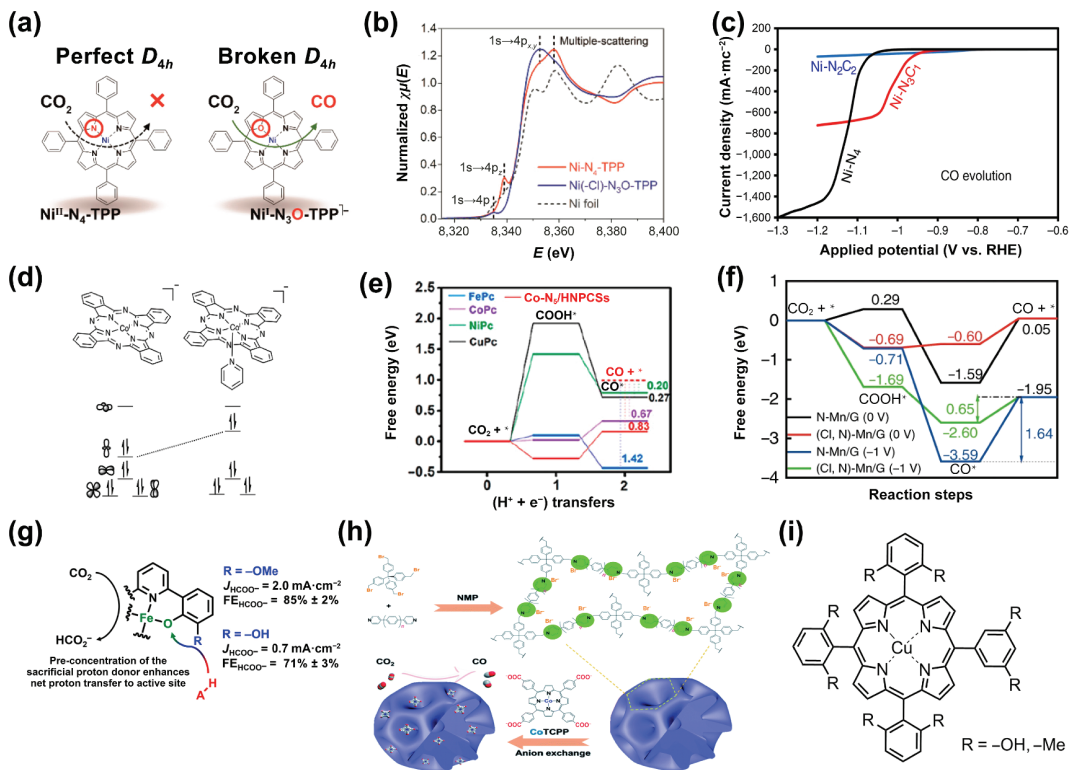


Figure 5 (a) Structure scheme of Ni-N₄-TPP and Ni(-Cl)-N₃O-TPP. (b) Ni K-edge XANES spectra of Ni-N₄-TPP, Ni(-Cl)-N₃O-TPP, and Ni foil. Reproduced with permission from Ref. [129], © American Chemical Society 2021. (c) Large partial current densities of CO in CO₂R on Ni-N₂C₂ (blue curve), Ni-N₃C₁ (red curve), and Ni-N₄ (black curve). Reproduced with permission from Ref. [130], © Hossain, D. et al. 2020. (d) Relative energies of the cobalt d orbitals in the 1 e⁻ reduced forms of CoPc and CoPc(py). The lower part of (d) is the energy increase of the cobalt d_{z²} orbital that results in the coordination of the axial pyridine. Reproduced with permission from Ref. [131], © The Royal Society of Chemistry 2016. (e) Calculated free energy diagram of CO₂R (red short dash line, the desorption free energy level of CO; dash dot lines, the desorption free energy of CO). Reproduced with permission from Ref. [132], © American Chemical Society 2018. (f) Calculated free energy of CO₂R on different catalysts. Reproduced with permission from Ref. [133], © Zhang, B. X. et al. 2019. (g) Scheme of electrocatalytic CO₂R to formate with molecular Fe(III) complexes containing pendent proton relays. Reproduced with permission from Ref. [135], © American Chemical Society 2020. (h) Schematic illustration of the synthesis of POP-Py(n) and POP-Py(n)/CoTCPP. Reproduced with permission from Ref. [137], © The Royal Society of Chemistry 2020. (i) Structure for copper-porphyrin molecule with 8 substituent groups.

interaction with CO_2 molecules and easier desorption of COOH^* and CO^* (Fig. 5(f)).

3.1.2 The outer-sphere interaction

Beyond the first-shell heteroatom coordination, the second-sphere interaction also plays an important role in tuning the catalytic performance [134]. The push-pull electronic effects of substituted groups can either increase or decrease the conversion of CO_2 . Nichols et al. proposed an outer-sphere effect by employing three differently substituted Fe(III) complexes as catalysts for electrochemical CO_2R [135]. The substituent with O atom showed a better current density for formate production than that of C atom, because O can preload the exogenous proton donor to the active sites. Compared to $-\text{OMe}$ group, $-\text{OH}$ group demonstrates a lower activity and selectivity probably owing to its partial or complete deprotonation during the reaction (Fig. 5(g)). Positively charged groups can stabilize the initial $\text{Fe}^{\circ}\text{-CO}_2$ adduct, and obtain a TOF as high as 10^6 s^{-1} at a low overpotential of 220 mV [136]. Tang et al. encapsulated anionic CoPc into a cationic porous polymer skeleton, and observed that the TOF increased three folds higher than the primitive anionic CoPc at $-0.6 \text{ V}_{\text{RHE}}$ [137]. *In-situ* surface-enhanced infrared absorption spectroscopy (SEIRAS) proved that positively-charged substitution can help to stabilize the CO_2^{*-} and weaken the Co-C bond, making CO desorption easier (Fig. 5(h)). Weng et al. prepared a molecular Cu catalyst substituted by $-\text{OH}$ which can convert CO_2 into methane, ethylene, and CO with total FEs of $\sim 50\%$ [138]. The control experiment of methyl-protected catalyst showed only 0.8% FE of formate and $< 28\%$ FE of CO (Fig. 5(i)). Wu et al. introduced four amino groups ($-\text{NH}_2$) to the β positions of CoPc ligand, which decreased the overpotential and increased the stability for methanol production [139]. Chen et al. encapsulated N-heterocyclic carbene (NHC)-ligated Cu-SAC into a Zr(IV) biphenyl dicarboxylate metal-organic framework, which can prevent the agglomeration of NHC-Cu, and finally achieved a methane FE of 81% at a current density of $420 \text{ mA}\cdot\text{cm}^{-2}$ [140]. Sun et al. introduced single P atoms into a N-doped carbon supported isolated Fe atom catalyst. The catalysts showed a CO FE of $\sim 97\%$ with a partial current density of $\sim 5 \text{ mA}\cdot\text{cm}^{-2}$ at an overpotential of 320 mV, and a superior Tafel slope of $59 \text{ mV}\cdot\text{dec}^{-1}$. DFT calculations proved that the single P atom in high coordination shells ($n \geq 3$) can enhance the electronic localization of Fe, which improved the stability of the key intermediate ${}^*\text{COOH}$, leading to an excellent CO_2R performance [141]. It is worth to mention that although the influence from the outer-sphere coordination environment is significant, the detailed mechanism is complicated and ambiguous at this moment so that further investigation remains required. Therefore, both the direct and indirect coordination environments of metal centers in SACs have a significant effect on the microscopic properties and catalytic performances. Precisely controlling the coordination environments of SACs is of great importance to improve the catalytic performance and reveal the structure-function correlation.

3.2 Conductive support effect

The charge transfer is an important factor that can influence the efficiency of electrochemical CO_2R . Generally speaking, conductive materials such as carbon allotropes, metals, and conductive polymers are most commonly-used supports for electrocatalytic reactions since rapid electrons transfer inside and/or on the surfaces of such materials can be realized, and thus facilitate electrochemical reactions on electrodes. Therefore, rational design of the support is critical important to improve catalytic performances of SACs.

Among the conductive supports already in use, carbon allotropes such as carbon black, graphene, carbon nanotubes (CNTs) [142], etc., are the most widely-applied materials in CO_2R due to their highly-conductive properties, large surface areas, and porous nanostructures. Ascribed to the highly-conjugated structures providing rich $\pi-\pi$ bonding, sp^2 -hybridized carbon (e.g., graphene, CNTs), and sp-hybridized carbon (e.g., graphdiyne (GDY)) have been applied as conductive substrates immobilizing SACs and hence boost the electrochemical CO_2R performance.

Wang's group has demonstrated a CoPc and carbon-based hybrid materials exhibiting extremely high selectivity over CO ($> 90\%$) across a wide range of potential meanwhile maintaining superb activities and stabilities [142]. The authors demonstrated that the abundant sp^2 -hybridized carbon in graphene reinforced the $\pi-\pi$ interaction between phthalocyanine coordinates in CoPc and repetitive graphitic units of CNTs, resulting in a well dispersion of CoPc molecules without aggregations. In contrast, the drop-casted CoPc on carbon fiber paper severely aggregated, leading to both poor activity and stability under the applied potential. It is convinced that a modest loading of CoPc can retain the single site morphology of CoPc molecules and thus hold an efficient electron transfer. The assembly strategy can be applied to a cyano-substituted CoPc/CNTs similarly, manifesting an over 95% FE of CO and a current density peaking at $15 \text{ mA}\cdot\text{cm}^{-2}$ (Fig. 6(a)). After that, several works on SACs followed the immobilization strategy with sp^2 carbon substrates. Liang and co-workers developed a defect-rich graphene (DrGO) anchoring CoPc molecules through strong $\pi-\pi$ interaction and achieved a peak FE of CO over 90.2% with a high current density of $73.9 \text{ mA}\cdot\text{cm}^{-2}$ [143]. Distinguished from pristine graphene and N-doped graphene, DrGO endows molecularly dispersed CoPc with a faster electron transfer from Co^{2+} to Co^+ and favorable adsorption of CO_2 molecules, resulting in a superior CO_2R performance.

Apart from sp^2 -hybridized carbon, GDY rich in both sp- and sp^2 -hybridized carbon has drawn marvelous attention as another type of carbon support for SACs in HER, OER, ORR, and CO_2R [144]. Liu et al. theoretically proved that Fe-SAC anchoring on GDY can catalyze CO_2 and promote the production of methane and ethanol [145]. They pointed out that the intense interaction between Fe center and GDY support via hybridization of Fe 3d and C 2p orbitals endowed the Fe-SAC with a more energetically preferred CO_2R process rather than HER. Further steps are taken to develop joint materials as more efficient support for SACs. Gu et al. reported a bottom-up synthesized sandwich-type catalyst in which the CoPc molecules (having CoN_4 sites) were finely dispersed on the GDY/G scaffold via van der Waals interaction, exhibiting an outstanding CO production [146]. Theoretical studies proved that the strong electronic interaction between CoPc and GDY stabilized the discrete CoN_4 center (Figs. 6(b) and 6(c)), and prevented CoPc agglomeration. Unlike random stacking of CoPc on pristine graphene, the specific adhesion of CoPc at diacetylenic linkages ($-\text{C}\equiv\text{C}-\text{C}\equiv\text{C}-$) of GDY showed a higher energy barrier of migration and intense interaction between Co 3d and π electron clouds. The sandwich-type CoPc/GDY/G facilitated the electron transfer from Co active centers to CO_2 molecules and lowered the energy barrier of the proton-transfer coupled electron transfer ($\text{CO}_2 + \text{H}^+ + \text{e}^- \rightarrow {}^*\text{COOH}$), resulting in a current density of $100 \text{ mA}\cdot\text{cm}^{-2}$ with a 97% FE of CO operating in a flow cell.

The manner of linkage and/or immobilization is another contributor to the charge transfer of SACs. Different from aforementioned SACs interacting with substrates through van der Waals interaction, covalent bonding such as axial coordination

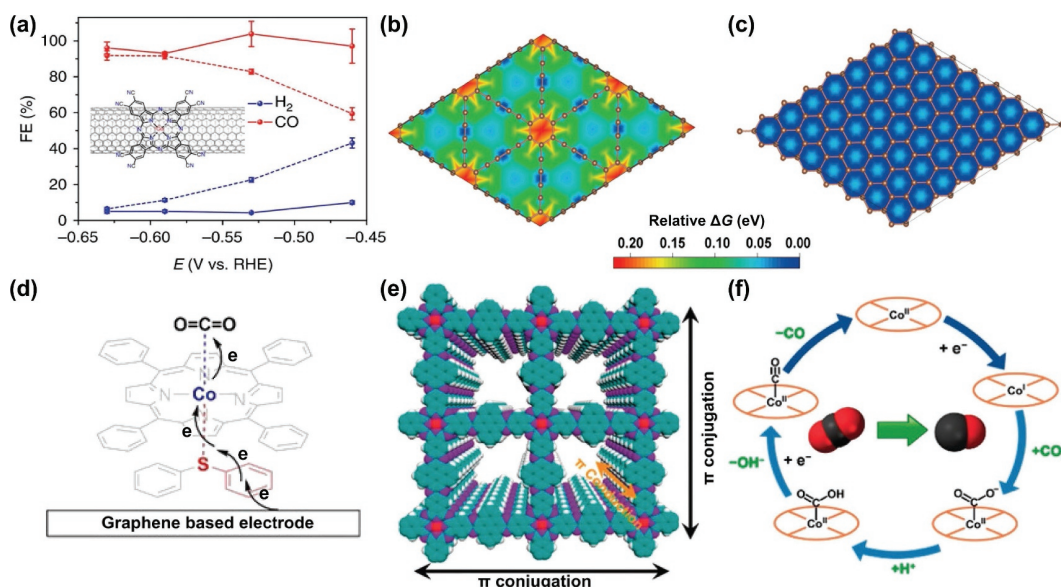


Figure 6 (a) FE of products at varied potentials on CoPc-CN/CNT (solid line) and CoPc/CNT (dotted line). Inset shows the molecular structure of CoPc-CN anchored on CNT. Reproduced with permission from Ref. [142], © Zhang X. et al. 2017. The potential energy surface maps of adsorbed CoPc molecules on GDY/G (b) and graphene (c). Reproduced with permission from Ref. [146], © American Chemical Society 2021. (d) Schematic illustration of PCo interacting with Di-S through the formation of axial Co-S bonds. Reproduced with permission from Ref. [147], © Wiley-VCH GmbH 2020. (e) The π structure of CoPc-PDQ-COF along the X, Y, and Z axis, which facilitates the electron transport to the catalytic center. (f) The possible catalytic mechanism of CO_2R on catalyst. Reproduced with permission from Ref. [148], © Wiley-VCH Verlag GmbH & Co. KGaA, Weinheim 2020.

bonding has an intense impact along the z axis, which facilitates the interfacial charge transfer. For example, Wang et al. modified tetraphenylporphyrin cobalt (PCo) with diphenyl sulfide (Di-S) as axial ligands to enhance the electron transfer from graphene to Co centers (Fig. 6(d)) [147]. In this way, the Di-S ligands interacted with graphene in a face-to-face fashion. In addition, the parallel stacking geometry of Di-S modified PCo on graphene endowed PCo with higher degree of dispersion, which induced an intense $\pi-\pi$ stacking that can facilitate the electron transfer. As a result, the activation of CO_2 molecules at Co sites was greatly enhanced, manifesting an increased TOF of CO higher than primitive PCo-G. In addition to coordinatively-incorporated SACs, Huang and co-workers developed a two-dimensional covalent organic framework (2D COFs) synthesized from CoPc and phenazine linkages (Figs. 6(e) and 6(f)) [148]. The highly-conjugated skeletons incorporated single Co sites, conductive π bonds, and chemically-stable covalent bonds together, largely increasing the activity (TOF = 11,412 h⁻¹) and selectivity (FE = 96%) for CO production with resistance to harsh conditions (acid, base, high temperature, etc.).

3.3 Synergistic and tandem system

Beyond the development of individual SACs as electrocatalysts for CO_2R , increasing attentions have been paid to those SACs combined with functionally-different catalysts such as other types of SACs [149], metal nanoparticles [150], metal nitrides [151], etc., that possess heteroatomic active centers. The incorporations of active centers of SACs and other catalysts that perform their own functions in CO_2R can remarkably boost the productivity by facilitating charge transfer and protonation process, improving local concentration of CO or even lowering the energy barrier of RDS. Accordingly, the introduction of heteronuclear or homonuclear metal atoms shows a great impact on the distribution of products (mainly CO) [149, 152] and/or generates further reduced products, such as hydrocarbons (methane and ethylene, etc.) [151, 153] and oxygenates (ethanol, etc.) [154].

Recently, works on synergistic catalysts for CO production have aroused great attention as the selectivity of CO can be tuned by rational design of neighboring metal centers. This synergistic

catalyst that comprises functionally-diverse metal centers can decrease the energy barrier of *COOH formation, a generally-recognized RDS in CO production. As a typical example of synergistic catalyst, a bimetallic 2D conjugated metal-organic framework loaded on CNTs is reported by Zhong et al., which manifests excellent performance of CO production (FE of 88%, TOF of 0.39 s⁻¹ at $-0.7 \text{ V}_{\text{RHE}}$) via synergistic interactions of ZnO_4 and CuN_4 [149]. The accumulation of protons at CuN_4 sites will promote the proton-coupled electron transfer of adsorbed CO_2 and thus lower down the barrier of *COOH formation at ZnO_4 sites, which ultimately facilitates the production of CO (Fig. 7(a)). The Bao's group reported a synergistic system promoting CO production using CoPc anchored on FeN sites as catalyst [152]. The addition of CoPc lowered the energy barrier of *CO desorption, but showed negligible effect on FeN sites so that the adsorption of *COOH at FeN sites was well maintained. The combination of Co and Fe bimetallic sites avoided the poisoning of *CO and suppressed HER. Consequently, the synergistic system exhibited an over 90 % FE of CO across a wide potential range (Fig. 7(b)). Zhang et al. constructed Pd₂ dual-atom site on acetylene black, which exhibited a superior CO_2R performance with a CO FE of 98.2% at $-0.85 \text{ V}_{\text{RHE}}$ far beyond that of Pd₁-SAC [155].

Beyond synergistic catalysts promoting CO production, efforts have been taken to seek for catalysts achieving a high yield of value-added fuels, including methane, ethylene, ethanol, etc. Previous computational and experimental studies have proven that bimetallic catalysts can break the linear scaling relationships on bare Cu in CO_2R and thus augment the selectivity of further reduced and more value-added products such as hydrocarbons and alcohols. This goal has been already achieved by tandem catalysis at bimetallic interfaces such as Cu/Ag [156], Cu/Zn [157], Cu/Au [158], etc. In these systems, the secondary metal is effective to buildup CO, which will subsequently immigrate to the neighboring Cu sites, and get reduced. Nevertheless, the high cost and large consumption of metals hinder the industry-scale application. Hence, the development of SACs with well-defined structures and highly-exposed active sites for tandem catalysis is urgently. On account of the pathways for $> 2\text{e}^-$ products, the

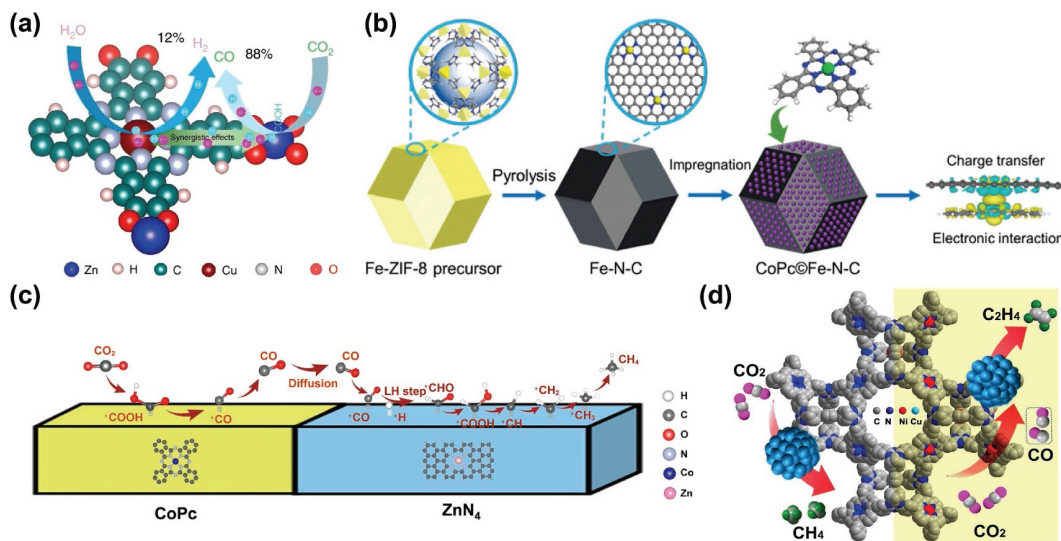


Figure 7 (a) Schematic HER and CO₂R process on P_cCu-O₈-Zn. Reproduced with permission from Ref. [149], © Zhong, H. X. et al. 2020. (b) Schematic preparation procedure of CoPc@Fe-N-C. The image on the far right is the calculated electron density difference of the CoPc@Fe-N-C structure. Blue and yellow contours present electron depletion and electron accumulation, respectively. Reproduced with permission from Ref. [152], © WILEY-VCH Verlag GmbH & Co. KGaA, Weinheim 2019. (c) A proposed reaction mechanism for CO₂R to produce CH₄ on CoPc@Zn-N-C. Reproduced with permission from Ref. [151], © Wiley-VCH GmbH 2020. (d) An illustration of isolated PTF(Ni) sites that can facilitate the C-C coupling to form ethylene on nearby Cu nanoparticles. Reproduced with permission from Ref. [153], © Wiley-VCH GmbH 2021.

*CO intermediates will undergo hydrogenation and/or C–C coupling, which indicates that SACs function individually is far from enough to generate reduced products other than CO and formate. For > 2e[−] C₁ products, the simultaneous adsorption of *H and *CO plays a key role in hydrogenation of *CO. Referring to bimetallic catalyst generating methane, the design of tandem SACs needs to take both spillover of CO and consequent hydrogenation process into account. Recently, Lin et al. designed a CoPc and Zn-N-C tandem catalyst for CO₂R [151] (Fig. 7(c)), attaining a FE of methane slightly lower than 20% with a maximum current density of 45 mA·cm^{−2}. Interestingly, they observed a favorable reaction pathway from CO₂ to methane occurred only when CoPc and Zn-N-C were integrated together as a tandem catalyst. It is speculated that the CO molecules generated at CoPc diffuse to the adjacent Zn-N-C surface, followed by the re-adsorption of CO molecules and consumption of pre-adsorbed *H. The two active species, *CO and *H subsequently follow the Langmuir–Hinshelwood mechanism to form *CHO, a key intermediate for hydrocarbon products and ultimately get reduced to methane.

Different from C₁ products, the promotion of C₂₊ products on SACs remains challenging since C–C coupling occurs merely at closely-located sites. In view of superb ability to produce CO by SACs, this class of SACs is a potential “CO spillover” catalyst that can be incorporated with Cu to enhance C–C coupling. This design concept of SACs-comprised tandem system mimics the previously reported work on Cu-based tandem systems. Sargent's group reported a tandem system combining Fe-SAC with Cu metal, achieving a 41% FE of ethanol with a partial current density of 124 mA·cm^{−2} at −0.82 V_{RHE}. The iron complex (FeTPP[Cl]) alone is evaluated to be a fairly good catalyst for CO production. As a result, the increased local CO concentration surrounding Cu promoted the chemisorption of *CO and lowered the energy barrier of consequent C–C coupling step [154]. Similarly, Meng et al. developed a tandem catalyst that integrated Ni-SAC and Cu nanoparticles to enhance C₂ production [153]. The adjoining Ni-SAC and nanostructured Cu sites facilitate the immigration of *in-situ* generated CO on Ni sites to the adjacent Cu [159, 160], where subsequent C–C coupling occurred. Ethylene with a FE larger than 50% at −1.1 V_{RHE} was attained (Fig. 7(d)).

4 Summary and perspective

The unique structures and electronic properties of SACs make them compelling in becoming a new frontier of electrochemical CO₂R research. Despite that significant progress in SACs development has been achieved, improvements in energy efficiency, selectivity, and long-term durability remain on the path toward their practical applications. To achieve this goal, the ingenious design of SACs should be considered, for accelerating the practical and widespread applications of CO₂R. We summarized a variety of strategies adopted in the reported studies to improve the activity, selectivity, and stability of SACs for CO₂R. Overall, the regulation of metal centers, first-shell, and second-sphere coordination environment, conductive supports and interface with a secondary catalyst were presented in details to promote CO₂R performance. Although SACs are a promising category of catalysts for CO₂R after decades of development, there remain many challenges that are yet to be addressed. Following are some aspects of current limitations and prospects for future development.

1. Expand the product scope of SACs for CO₂R. As summarized in this review, most SACs mainly produce CO and formate, and their selectivities towards hydrocarbons and oxygenates are much lower compared with those of nanoparticle counterparts and are far from the desirable target for practical applications. Expanding the product scope of SACs is crucial but remains very challenging. Interfacing SACs with another functionally-different catalyst to construct a tandem catalytic system is a promising way to address this issue [161]. Beyond that, to overcome the geometrical limitation of C–C coupling on isolated metal centers, atomic dual-metal or tri-metal sites may also open up more opportunities for CO₂R into C₂₊ fuels, where more than one active center is demanded to create synergistic interactions. To achieve these goals, further advances in synthesis approaches are needed.

2. Rational design of SACs under the guidance of simulation. Theoretical modeling of electrochemical interface is an important strategy to predict the reaction pathways and identify the key active site motifs, multiple intermediates, and intrinsic descriptors for catalysis. However, it is notable that more efforts to date laid on analyzing the reaction energetics thermodynamically, further developments of kinetic modeling will be great helpful to better

understand the interplay among the electronic structure of catalyst, adsorbate coverage and interactions, potential-dependent activation energy, and pH effects. The positive side is that active sites on SACs are uniform and homogeneous, unlike most heterogeneous electrocatalysts. Therefore, theoretical modelling should be more clear and easier to perform than the conventional system. Beyond that, the diverse properties of metal centers and various intermediates in CO₂R cause the experimental screening of SACs mostly in a trial-and-error way, which is very time consuming. The advanced numerical calculation technique, such as machine-learning algorithms, presents a promising opportunity to establish stronger predictive capabilities and screening methods, which can save catalyst screening efforts and promote the rational design of highly efficient SACs. Moreover, the multiscale modeling of reactant (e.g., CO₂) feeding and mass transport will be also critical for a better understanding of interfacial catalysis, in particular for the practical high surface area SACs and vapor-fed reactors.

3. *Operando* technique development. *In-situ* tracking the reaction intermediates and evolution of active sites under operating conditions is crucial to understand the reaction mechanism and further optimize the performance of SACs. However, it is challenging to design *in-situ* spectroscopy experiments to ensure the attained spectra are solely from the single active sites. Although multiple *operando* characterization techniques have been implemented for CO₂R studies, providing new insights [162], there are more can be done to broaden the capability of currently available techniques. For instance, *in-situ* time-resolved spectroscopic techniques to monitor the dynamic surface chemistry of intermediates on SACs are seldomly reported. These will be invaluable tools for offering better understanding of active sites, elucidation of reaction mechanisms, and validation of predictions from theoretical modeling.

4. Gas-fed reactor implementation. Apart from the fundamental structure designing, it is also demanded to develop reactor systems to enable scalable, selective, low-cost, and energy efficient CO₂ conversion to value-added fuels. Practical electrochemical CO₂R requires electrochemical devices to operate at a large current density higher than 150 mA·cm⁻², whereas most of the SACs catalysts, to date, operate at a low current density < 30 mA·cm⁻² because of the mass transfer limitation of CO₂ in aqueous media [163]. Most notably, significant progress has been made in recent years in development of gas diffusion electrode, which significantly reduces the diffusion path length of CO₂ to catalyst surface and increases CO₂ availability for a high reaction rate. For example, Sargent's group showed a partial current density for C₂₊ of 1.21 A·cm⁻², which was up to 45% half-cell energy efficiency in flow-cell [164]. Wang et al. report an extremely-high current density of 1.6 A·cm⁻² with a C₂₊ FE of 80% for CO₂R in a flow cell [165]. In this regard, while there is always a need for fundamental research, we are at a stage that to start accelerating practical device development. This includes optimization of device components (e.g., working electrode, membrane, cell geometry, etc.) and conditions (e.g., pH, gas feeding, electrolyte flow rate, etc.), and testing the tolerance to more realistic conditions. For instance, renewable energy powered CO₂R may suffer from an interrupted power input due to the intermittent energy supply, such as wind and solar, so tolerance to these factors should be seriously taken into account for future large-scale deployment of CO₂R technologies.

Overall, as a new star category of catalyst, SACs have experienced explosive growth and demonstrated their unique advantages as model catalysts for CO₂R in the fast few years. We believe that with continued research efforts devoted, more promising developments of highly active, selective, and robust

SACs for CO₂R will be realized in the near future, bringing the world closer towards a closed-loop anthropogenic carbon cycle.

Acknowledgment

This research was supported by the National Natural Science Foundation of China (Nos. 21872039 and 22072030) and Science and Technology Commission of Shanghai Municipality (Nos. 18JC1411700 and 19DZ2270100).

References

- [1] Caldeira, K.; Wickett, M. E. Anthropogenic carbon and ocean pH. *Nature* **2003**, *425*, 365.
- [2] Chu, S.; Majumdar, A. Opportunities and challenges for a sustainable energy future. *Nature* **2012**, *488*, 294–303.
- [3] Shakun, J. D.; Clark, P. U.; He, F.; Marcott, S. A.; Mix, A. C.; Liu, Z. Y.; Otto-Bliesner, B.; Schmittner, A.; Bard, E. Global warming preceded by increasing carbon dioxide concentrations during the last deglaciation. *Nature* **2012**, *484*, 49–54.
- [4] Kondratenko, E. V.; Mul, G.; Baltrusaitis, J.; Larrazabal, G. O.; Pérez-Ramírez, J. Status and perspectives of CO₂ conversion into fuels and chemicals by catalytic, photocatalytic and electrocatalytic processes. *Energy Environ. Sci.* **2013**, *6*, 3112–3135.
- [5] Nitopi, S.; Bertheussen, E.; Scott, S. B.; Liu, X. Y.; Engstfeld, A. K.; Horch, S.; Seger, B.; Stephens, I. E. L.; Chan, K.; Hahn, C. et al. Progress and perspectives of electrochemical CO₂ reduction on copper in aqueous electrolyte. *Chem. Rev.* **2019**, *119*, 7610–7672.
- [6] Ross, M. B.; De Luna, P.; Li, Y. F.; Dinh, C. T.; Kim, D.; Yang, P.; Sargent, E. H. Designing materials for electrochemical carbon dioxide recycling. *Nat. Catal.* **2019**, *2*, 648–658.
- [7] Grim, R. G.; Huang, Z.; Guarneri, M. T.; Ferrell III, J. R.; Tao, L.; Schaidle, J. A. Transforming the carbon economy: Challenges and opportunities in the convergence of low-cost electricity and reductive CO₂ utilization. *Energy Environ. Sci.* **2020**, *13*, 472–494.
- [8] Kulkarni, A. P.; Hos, T.; Landau, M. V.; Fini, D.; Gidley, S.; Herskowitz, M. Techno-economic analysis of a sustainable process for converting CO₂ and H₂O to feedstock for fuels and chemicals. *Sustainable Energy Fuels* **2021**, *5*, 486–500.
- [9] Sharifian, R.; Wagterveld, R. M.; Digdaya, I. A.; Xiang, C.; Vermaas, D. A. Electrochemical carbon dioxide capture to close the carbon cycle. *Energy Environ. Sci.* **2021**, *14*, 781–814.
- [10] Chen, C.; Khosrowabadi Kotyk, J. F.; Sheehan, S. W. Progress toward commercial application of electrochemical carbon dioxide reduction. *Chem* **2018**, *4*, 2571–2586.
- [11] Kortlever, R.; Shen, J.; Schouten, K. J. P.; Calle-Vallejo, F.; Koper, M. T. M. Catalysts and reaction pathways for the electrochemical reduction of carbon dioxide. *J. Phys. Chem. Lett.* **2015**, *6*, 4073–4082.
- [12] Qiao, J. L.; Liu, Y. Y.; Hong, F.; Zhang, J. J. A review of catalysts for the electroreduction of carbon dioxide to produce low-carbon fuels. *Chem. Soc. Rev.* **2014**, *43*, 631–675.
- [13] Ringe, S.; Clark, E. L.; Resasco, J.; Walton, A.; Seger, B.; Bell, A. T.; Chan, K. Understanding cation effects in electrochemical CO₂ reduction. *Energy Environ. Sci.* **2019**, *12*, 3001–3014.
- [14] Yoshio, H.; Katsuhei, K.; Shin, S. Production of CO and CH₄ in electrochemical reduction of CO₂ at metal electrodes in aqueous hydrogencarbonate solution. *Chem. Lett.* **1985**, *14*, 1695–1698.
- [15] Birdja, Y. Y.; Pérez-Gallent, E.; Figueiredo, M. C.; Göttle, A. J.; Calle-Vallejo, F.; Koper, M. T. M. Advances and challenges in understanding the electrocatalytic conversion of carbon dioxide to fuels. *Nat. Energy* **2019**, *4*, 732–745.
- [16] Benson, E. E.; Kubiak, C. P.; Sathrum, A. J.; Smieja, J. M. Electrocatalytic and homogeneous approaches to conversion of CO₂ to liquid fuels. *Chem. Soc. Rev.* **2009**, *38*, 89–99.
- [17] Franco, F.; Rettenmaier, C.; Jeon, H. S.; Roldan Cuenya, B. Transition metal-based catalysts for the electrochemical CO₂ reduction: From atoms and molecules to nanostructured materials.

- Chem. Soc. Rev.* **2020**, *49*, 6884–6946.
- [18] Raciti, D.; Wang, C. Recent advances in CO₂ reduction electrocatalysis on copper. *ACS Energy Lett.* **2018**, *3*, 1545–1556.
- [19] Vasileff, A.; Xu, C. C.; Jiao, Y.; Zheng, Y.; Qiao, S. Z. Surface and interface engineering in copper-based bimetallic materials for selective CO₂ electroreduction. *Chem* **2018**, *4*, 1809–1831.
- [20] Zhang, S.; Fan, Q.; Xia, R.; Meyer, T. J. CO₂ reduction: From homogeneous to heterogeneous electrocatalysis. *Acc. Chem. Res.* **2020**, *53*, 255–264.
- [21] Wang, Y. C.; Xu, L.; Zhan, L. S.; Yang, P. Y.; Tang, S. H.; Liu, M. J.; Zhao, X.; Xiong, Y.; Chen, Z. Y.; Lei, Y. P. Electron accumulation enables Bi efficient CO₂ reduction for formate production to boost clean Zn-CO₂ batteries. *Nano Energy* **2022**, *92*, 106780.
- [22] Wang, A. Q.; Li, J.; Zhang, T. Heterogeneous single-atom catalysis. *Nat. Rev. Chem.* **2018**, *2*, 65–81.
- [23] Zhang, L. L.; Ren, Y. J.; Liu, W. G.; Wang, A. Q.; Zhang, T. Single-atom catalyst: A rising star for green synthesis of fine chemicals. *Natl. Sci. Rev.* **2018**, *5*, 653–672.
- [24] Zhang, F. F.; Zhu, Y. L.; Lin, Q.; Zhang, L.; Zhang, X. W.; Wang, H. Y. Noble-metal single-atoms in thermocatalysis, electrocatalysis, and photocatalysis. *Energy Environ. Sci.* **2021**, *14*, 2954–3009.
- [25] Zhang, L. L.; Zhou, M. X.; Wang, A. Q.; Zhang, T. Selective hydrogenation over supported metal catalysts: From nanoparticles to single atoms. *Chem. Rev.* **2020**, *120*, 683–733.
- [26] Zhao, D.; Zhuang, Z. W.; Cao, X.; Zhang, C.; Peng, Q.; Chen, C.; Li, Y. D. Atomic site electrocatalysts for water splitting, oxygen reduction and selective oxidation. *Chem. Soc. Rev.* **2020**, *49*, 2215–2264.
- [27] Ji, S. F.; Chen, Y. J.; Wang, X. L.; Zhang, Z. D.; Wang, D. S.; Li, Y. D. Chemical synthesis of single atomic site catalysts. *Chem. Rev.* **2020**, *120*, 11900–11955.
- [28] Li, Z.; Ji, S. F.; Liu, Y. W.; Cao, X.; Tian, S. B.; Chen, Y. J.; Niu, Z. Q.; Li, Y. D. Well-defined materials for heterogeneous catalysis: From nanoparticles to isolated single-atom sites. *Chem. Rev.* **2020**, *120*, 623–682.
- [29] Qiao, B. T.; Wang, A. Q.; Yang, X. F.; Allard, L. F.; Jiang, Z.; Cui, Y. T.; Liu, J. Y.; Li, J.; Zhang, T. Single-atom catalysis of CO oxidation using Pt₁/FeO_x. *Nat. Chem.* **2011**, *3*, 634–641.
- [30] Lang, R.; Du, X. R.; Huang, Y. K.; Jiang, X. Z.; Zhang, Q.; Guo, Y. L.; Liu, K. P.; Qiao, B. T.; Wang, A. Q.; Zhang, T. Single-atom catalysts based on the metal–oxide interaction. *Chem. Rev.* **2020**, *120*, 11986–12043.
- [31] Li, X. N.; Yang, X. F.; Zhang, J. M.; Huang, Y. Q.; Liu, B. *In situ/operando* techniques for characterization of single-atom catalysts. *ACS Catal.* **2019**, *9*, 2521–2531.
- [32] Ye, C. L.; Zhang, N. Q.; Wang, D. S.; Li, Y. F. Single atomic site catalysts: Synthesis, characterization, and applications. *Chem. Commun.* **2020**, *56*, 7687–7697.
- [33] Tian, S. B.; Gong, W. B.; Chen, W. X.; Lin, N.; Zhu, Y. Q.; Feng, Q. C.; Xu, Q.; Fu, Q.; Chen, C.; Luo, J. et al. Regulating the catalytic performance of single-atomic-site Ir catalyst for biomass conversion by metal-support interactions. *ACS Catal.* **2019**, *9*, 5223–5230.
- [34] Tian, S. B.; Wang, Z. Y.; Gong, W. B.; Chen, W. X.; Feng, Q. C.; Xu, Q.; Chen, C.; Chen, C.; Peng, Q.; Gu, L. et al. Temperature-controlled selectivity of hydrogenation and hydrodeoxygenation in the conversion of biomass molecule by the Ru₁/mpg-C₃N₄ catalyst. *J. Am. Chem. Soc.* **2018**, *140*, 11161–11164.
- [35] Wei, S. J.; Li, A.; Liu, J. C.; Li, Z.; Chen, W. X.; Gong, Y.; Zhang, Q. H.; Cheong, W. C.; Wang, Y.; Zheng, L. R. et al. Direct observation of noble metal nanoparticles transforming to thermally stable single atoms. *Nat. Nanotechnol.* **2018**, *13*, 856–861.
- [36] Ye, X.; Yang, C. Y.; Pan, X. L.; Ma, J. G.; Zhang, Y. R.; Ren, Y. J.; Liu, X. Y.; Li, L.; Huang, Y. Q. Highly selective hydrogenation of CO₂ to ethanol via designed bifunctional Ir₁-In₂O₃ single-atom catalyst. *J. Am. Chem. Soc.* **2020**, *142*, 19001–19005.
- [37] Liu, H.; Li, X. X.; Ma, Z. H.; Sun, M. Z.; Li, M. G.; Zhang, Z. Y.; Zhang, L.; Tang, Z. B.; Yao, Y.; Huang, B. L. et al. Atomically dispersed Cu catalyst for efficient chemoselective hydrogenation reaction. *Nano Lett.* **2021**, *21*, 10284–10291.
- [38] Liu, Y.; Liu, J. C.; Li, T. H.; Duan, Z. H.; Zhang, T. Y.; Yan, M.; Li, W. L.; Xiao, H.; Wang, Y. G.; Chang, C. R. et al. Unravelling the enigma of nonoxidative conversion of methane on iron single-atom catalysts. *Angew. Chem., Int. Ed.* **2020**, *59*, 18586–18590.
- [39] Sun, X. H.; Olivos-Suarez, A. I.; Osadchii, D.; Romero, M. J. V.; Kapteijn, F.; Gascon, J. Single cobalt sites in mesoporous N-doped carbon matrix for selective catalytic hydrogenation of nitroarenes. *J. Catal.* **2018**, *357*, 20–28.
- [40] Yang, J. R.; Zeng, D. Q.; Zhang, Q. G.; Cui, R. F.; Hassan, M.; Dong, L. Q.; Li, J.; He, Y. L. Single Mn atom anchored on N-doped porous carbon as highly efficient Fenton-like catalyst for the degradation of organic contaminants. *Appl. Catal. B: Environ.* **2020**, *279*, 119363.
- [41] Zuo, Z. J.; Liu, S. Z.; Wang, Z. C.; Liu, C.; Huang, W.; Huang, J.; Liu, P. Dry reforming of methane on single-site Ni/MgO catalysts: Importance of site confinement. *ACS Catal.* **2018**, *8*, 9821–9835.
- [42] Fu, J. H.; Dong, J. H.; Si, R.; Sun, K. J.; Zhang, J. Y.; Li, M. R.; Yu, N. N.; Zhang, B. S.; Humphrey, M. G.; Fu, Q. et al. Synergistic effects for enhanced catalysis in a dual single-atom catalyst. *ACS Catal.* **2021**, *11*, 1952–1961.
- [43] Gu, X. K.; Qiao, B. T.; Huang, C. Q.; Ding, W. C.; Sun, K. J.; Zhan, E. S.; Zhang, T.; Liu, J. Y.; Li, W. X. Supported single Pt₁/Au₁ atoms for methanol steam reforming. *ACS Catal.* **2014**, *4*, 3886–3890.
- [44] Sun, G. D.; Zhao, Z. J.; Mu, R. T.; Zha, S. J.; Li, L. L.; Chen, S.; Zang, K. T.; Luo, J.; Li, Z. L.; Purdy, S. C. et al. Breaking the scaling relationship via thermally stable Pt/Cu single atom alloys for catalytic dehydrogenation. *Nat. Commun.* **2018**, *9*, 4454.
- [45] Tang, Y.; Wei, Y. C.; Wang, Z. Y.; Zhang, S. R.; Li, Y. T.; Nguyen, L.; Li, Y. X.; Zhou, Y.; Shen, W. J.; Tao, F. F. et al. Synergy of single-atom Ni₁ and Ru₁ sites on CeO₂ for dry reforming of CH₄. *J. Am. Chem. Soc.* **2019**, *141*, 7283–7293.
- [46] Zhou, P.; Hou, X. G.; Chao, Y. G.; Yang, W. X.; Zhang, W. Y.; Mu, Z. J.; Lai, J. P.; Lv, F.; Yang, K.; Liu, Y. X. et al. Synergetic interaction between neighboring platinum and ruthenium monomers boosts CO oxidation. *Chem. Sci.* **2019**, *10*, 5898–5905.
- [47] Chen, Y.; Ji, S. F.; Chen, C.; Peng, Q.; Wang, D. S.; Li, Y. D. Single-atom catalysts: Synthetic strategies and electrochemical applications. *Joule* **2018**, *2*, 1242–1264.
- [48] Lu, B. Z.; Liu, Q. M.; Chen, S. W. Electrocatalysis of single-atom sites: Impacts of atomic coordination. *ACS Catal.* **2020**, *10*, 7584–7618.
- [49] Nguyen, T. N.; Salehi, M.; Van Le, Q.; Seifitokaldani, A.; Dinh, C. T. Fundamentals of electrochemical CO₂ reduction on single-metal-atom catalysts. *ACS Catal.* **2020**, *10*, 10068–10095.
- [50] Ou, H. H.; Wang, D. S.; Li, Y. D. How to select effective electrocatalysts: Nano or single atom? *Nano Select* **2021**, *2*, 492–511.
- [51] Peng, Y.; Lu, B. Z.; Chen, S. W. Carbon-supported single atom catalysts for electrochemical energy conversion and storage. *Adv. Mater.* **2018**, *30*, 1801995.
- [52] Wang, Y. X.; Su, H. Y.; He, Y. H.; Li, L. G.; Zhu, S. Q.; Shen, H.; Xie, P. F.; Fu, X. B.; Zhou, G. Y.; Feng, C. et al. Advanced electrocatalysts with single-metal-atom active sites. *Chem. Rev.* **2020**, *120*, 12217–12314.
- [53] Zhang, H. B.; Cheng, W. R.; Luan, D. Y.; Lou, X. W. Atomically dispersed reactive centers for electrocatalytic CO₂ reduction and water splitting. *Angew. Chem., Int. Ed.* **2021**, *60*, 13177–13196.
- [54] Zhang, Q. Q.; Guan, J. Q. Single-atom catalysts for electrocatalytic applications. *Adv. Funct. Mater.* **2020**, *30*, 2000768.
- [55] Liu, M. M.; Wang, L. L.; Zhao, K. N.; Shi, S. S.; Shao, Q. S.; Zhang, L.; Sun, X. L.; Zhao, Y. F.; Zhang, J. J. Atomically dispersed metal catalysts for the oxygen reduction reaction: Synthesis, characterization, reaction mechanisms and electrochemical energy applications. *Energy Environ. Sci.* **2019**, *12*, 2890–2923.

- [56] Jing, H. Y.; Zhu, P.; Zheng, X. B.; Zhang, Z. D.; Wang, D. S.; Li, Y. D. Theory-oriented screening and discovery of advanced energy transformation materials in electrocatalysis. *Adv. Powder Mater.*, in press, <https://doi.org/10.1016/j.apmate.2021.10.004>.
- [57] Wang, Y.; Zheng, X. B.; Wang, D. S. Design concept for electrocatalysts. *Nano Res.* **2022**, *15*, 1730–1752.
- [58] Wang, Y. C.; Liu, Y.; Liu, W.; Wu, J.; Li, Q.; Feng, Q. G.; Chen, Z. Y.; Xiong, X.; Wang, D. S.; Lei, Y. P. Regulating the coordination structure of metal single atoms for efficient electrocatalytic CO₂ reduction. *Energy Environ. Sci.* **2020**, *13*, 4609–4624.
- [59] Zhou, D. N.; Li, X. Y.; Shang, H. S.; Qin, F. J.; Chen, W. X. Atomic regulation of metal-organic framework derived carbon-based single-atom catalysts for the electrochemical CO₂ reduction reaction. *J. Mater. Chem. A* **2021**, *9*, 23382–23418.
- [60] Lu, X. L.; Rong, X.; Zhang, C.; Lu, T. B. Carbon-based single-atom catalysts for CO₂ electroreduction: Progress and optimization strategies. *J. Mater. Chem. A* **2020**, *8*, 10695–10708.
- [61] Peterson, A. A.; Abild-Pedersen, F.; Studt, F.; Rossmeisl, J.; Nørskov, J. K. How copper catalyzes the electroreduction of carbon dioxide into hydrocarbon fuels. *Energy Environ. Sci.* **2010**, *3*, 1311–1315.
- [62] Wang, Y. F.; Chen, Z.; Han, P.; Du, Y. H.; Gu, Z. X.; Xu, X.; Zheng, G. F. Single-atomic Cu with multiple oxygen vacancies on ceria for electrocatalytic CO₂ reduction to CH₄. *ACS Catal.* **2018**, *8*, 7113–7119.
- [63] Zhang, Y.; Dong, L.-Z.; Li, S.; Huang, X.; Chang, J.-N.; Wang, J.-H.; Zhou, J.; Li, S.-L.; Lan, Y.-Q. Coordination environment dependent selectivity of single-site-Cu enriched crystalline porous catalysts in CO₂ reduction to CH₄. *Nature Commun.* **2021**, *12*, 6390.
- [64] Wang, G. X.; Chen, J. X.; Ding, Y. C.; Cai, P. W.; Yi, L. C.; Li, Y.; Tu, C. Y.; Hou, Y.; Wen, Z. H.; Dai, L. M. Electrocatalysis for CO₂ conversion: From fundamentals to value-added products. *Chem. Soc. Rev.* **2021**, *50*, 4993–5061.
- [65] Zhao, K.; Quan, X. Carbon-based materials for electrochemical reduction of CO₂ to C₂₊ oxygenates: Recent progress and remaining challenges. *ACS Catal.* **2021**, *11*, 2076–2097.
- [66] Landers, A. T.; Fields, M.; Torelli, D. A.; Xiao, J. P.; Hellstern, T. R.; Francis, S. A.; Tsai, C.; Kibsgaard, J.; Lewis, N. S.; Chan, K. et al. The predominance of hydrogen evolution on transition metal sulfides and phosphides under CO₂ reduction conditions: An experimental and theoretical study. *ACS Energy Lett.* **2018**, *3*, 1450–1457.
- [67] Goyal, A.; Marcandalli, G.; Mints, V. A.; Koper, M. T. M. Competition between CO₂ reduction and hydrogen evolution on a gold electrode under well-defined mass transport conditions. *J. Am. Chem. Soc.* **2020**, *142*, 4154–4161.
- [68] Kimura, K. W.; Casebolt, R.; Cimada DaSilva, J.; Kauffman, E.; Kim, J.; Dunbar, T. A.; Pollock, C. J.; Suntivich, J.; Hanrath, T. Selective electrochemical CO₂ reduction during pulsed potential stems from dynamic interface. *ACS Catal.* **2020**, *10*, 8632–8639.
- [69] Gattrell, M.; Gupta, N.; Co, A. A review of the aqueous electrochemical reduction of CO₂ to hydrocarbons at copper. *J. Electroanal. Chem.* **2006**, *594*, 1–19.
- [70] Baruch, M. F.; Pander III, J. E.; White, J. L.; Bocarsly, A. B. Mechanistic insights into the reduction of CO₂ on tin electrodes using *in situ* ATR-IR spectroscopy. *ACS Catal.* **2015**, *5*, 3148–3156.
- [71] Gao, D. F.; Zhou, H.; Cai, F.; Wang, D. N.; Hu, Y. F.; Jiang, B.; Cai, W. B.; Chen, X. Q.; Si, R.; Yang, F. et al. Switchable CO₂ electroreduction via engineering active phases of Pd nanoparticles. *Nano Res.* **2017**, *10*, 2181–2191.
- [72] Zhao, Y. R.; Chang, X. X.; Malkani, A. S.; Yang, X.; Thompson, L.; Jiao, F.; Xu, B. J. Speciation of Cu surfaces during the electrochemical CO reduction reaction. *J. Am. Chem. Soc.* **2020**, *142*, 9735–9743.
- [73] Surdhar, P. S.; Mezyk, S. P.; Armstrong, D. A. Reduction potential of the carboxyl radical anion in aqueous solutions. *J. Phys. Chem.* **1989**, *93*, 3360–3363.
- [74] Rosen, B. A.; Salehi-Khojin, A.; Thorson, M. R.; Zhu, W.; Whipple, D. T.; Kenis, P. J. A.; Masel, R. I. Ionic liquid-mediated selective conversion of CO₂ to CO at low overpotentials. *Science* **2011**, *334*, 643–644.
- [75] Sun, Z. Y.; Ma, T.; Tao, H. C.; Fan, Q.; Han, B. X. Fundamentals and challenges of electrochemical CO₂ reduction using two-dimensional materials. *Chem.* **2017**, *3*, 560–587.
- [76] Rosen, J.; Hutchings, G. S.; Lu, Q.; Rivera, S.; Zhou, Y.; Vlachos, D. G.; Jiao, F. Mechanistic insights into the electrochemical reduction of CO₂ to CO on nanostructured Ag surfaces. *ACS Catal.* **2015**, *5*, 4293–4299.
- [77] Ju, W.; Bagger, A.; Hao, G. P.; Varela, A. S.; Sinev, I.; Bon, V.; Roldan Cuenya, B.; Kaskel, S.; Rossmeisl, J.; Strasser, P. Understanding activity and selectivity of metal-nitrogen-doped carbon catalysts for electrochemical reduction of CO₂. *Nat. Commun.* **2017**, *8*, 944.
- [78] Todorova, T. K.; Schreiber, M. W.; Fontecave, M. Mechanistic understanding of CO₂ reduction reaction (CO₂RR) toward multicarbon products by heterogeneous copper-based catalysts. *ACS Catal.* **2020**, *10*, 1754–1768.
- [79] Vijay, S.; Ju, W.; Brückner, S.; Tsang, S. C.; Strasser, P.; Chan, K. Unified mechanistic understanding of CO₂ reduction to CO on transition metal and single atom catalysts. *Nat. Catal.* **2021**, *4*, 1024–1031.
- [80] Smith, B. D.; Irish, D. E.; Kedzierzawski, P.; Augustynski, J. A surface enhanced roman scattering study of the intermediate and poisoning species formed during the electrochemical reduction of CO₂ on copper. *J. Electrochem. Soc.* **1997**, *144*, 4288–4296.
- [81] Qin, X. P.; Zhu, S. Q.; Xiao, F.; Zhang, L. L.; Shao, M. H. Active sites on heterogeneous single-iron-atom electrocatalysts in CO₂ reduction reaction. *ACS Energy Lett.* **2019**, *4*, 1778–1783.
- [82] Fan, Q.; Hou, P. F.; Choi, C.; Wu, T. S.; Hong, S.; Li, F.; Soo, Y. L.; Kang, P.; Jung, Y.; Sun, Z. Y. Activation of Ni particles into single Ni-N atoms for efficient electrochemical reduction of CO₂. *Adv. Energy Mater.* **2020**, *10*, 1903068.
- [83] Meshitsuka, S.; Ichikawa, M.; Tamaru, K. Electrocatalysis by metal phthalocyanines in the reduction of carbon dioxide. *J. Chem. Soc., Chem. Commun.* **1974**, 158–159.
- [84] Kazuya, H.; Katsuhiro, T.; Hideo, S.; Shinobu, T. Electrocatalytic behavior of tetrasulfonated metal phthalocyanines in the reduction of carbon dioxide. *Chem. Lett.* **1977**, *6*, 1137–1140.
- [85] Katsuhiro, T.; Kazuya, H.; Hideo, S.; Shinobu, T. Electrocatalytic behavior of metal porphyrins in the reduction of carbon dioxide. *Chem. Lett.* **1979**, *8*, 305–308.
- [86] Fisher, B. J.; Eisenberg, R. Electrocatalytic reduction of carbon dioxide by using macrocycles of nickel and cobalt. *J. Am. Chem. Soc.* **1980**, *102*, 7361–7363.
- [87] Lin, S.; Diercks, C. S.; Zhang, Y. B.; Kornienko, N.; Nichols, E. M.; Zhao, Y. B.; Paris, A. R.; Kim, D.; Yang, P. D.; Yaghi, O. M. et al. Covalent organic frameworks comprising cobalt porphyrins for catalytic CO₂ reduction in water. *Science* **2015**, *349*, 1208–1213.
- [88] Chen, B. T.; Li, B. R.; Tian, Z. Q.; Liu, W. B.; Liu, W. P.; Sun, W. W.; Wang, K.; Chen, L.; Jiang, J. Z. Enhancement of mass transfer for facilitating industrial-level CO₂ electroreduction on atomic Ni-N₄ sites. *Adv. Energy Mater.* **2021**, *11*, 2102152.
- [89] Ni, W. P.; Liu, Z. X.; Zhang, Y.; Ma, C.; Deng, H. Q.; Zhang, S. G.; Wang, S. Y. Electroreduction of carbon dioxide driven by the intrinsic defects in the carbon plane of a single Fe-N₄ site. *Adv. Mater.* **2021**, *33*, 2003238.
- [90] Li, X. G.; Xi, S. B.; Sun, L. B.; Dou, S.; Huang, Z. F.; Su, T.; Wang, X. Isolated FeN₄ sites for efficient electrocatalytic CO₂ reduction. *Adv. Sci.* **2020**, *7*, 2001545.
- [91] Grasemann, M.; Laurenczy, G. Formic acid as a hydrogen source—recent developments and future trends. *Energy Environ. Sci.* **2012**, *5*, 8171–8181.
- [92] Pan, Z. W. H.; Wang, K.; Ye, K. H.; Wang, Y.; Su, H. Y.; Hu, B. H.; Xiao, J.; Yu, T. W.; Wang, Y.; Song, S. Q. Intermediate adsorption states switch to selectively catalyze electrochemical CO₂

- reduction. *ACS Catal.* **2020**, *10*, 3871–3880.
- [93] Li, L.; Ozden, A.; Guo, S. Y.; García de Arquer, F. P.; Wang, C. H.; Zhang, M. Z.; Zhang, J.; Jiang, H. Y.; Wang, W.; Dong, H. et al. Stable, active CO₂ reduction to formate via redox-modulated stabilization of active sites. *Nat. Commun.* **2021**, *12*, 5223.
- [94] Huang, P. C.; Cheng, M.; Zhang, H. H.; Zuo, M.; Xiao, C.; Xie, Y. Single Mo atom realized enhanced CO₂ electro-reduction into formate on N-doped graphene. *Nano Energy* **2019**, *61*, 428–434.
- [95] Shang, H. S.; Wang, T.; Pei, J. J.; Jiang, Z. L.; Zhou, D. N.; Wang, Y.; Li, H. J.; Dong, J. C.; Zhuang, Z. B.; Chen, W. X. et al. Design of a single-atom indium³⁺-N₄ interface for efficient electroreduction of CO₂ to formate. *Angew. Chem., Int. Ed.* **2020**, *59*, 22465–22469.
- [96] Zu, X. L.; Li, X. D.; Liu, W.; Sun, Y. F.; Xu, J. Q.; Yao, T.; Yan, W. S.; Gao, S.; Wang, C. M.; Wei, S. Q. et al. Efficient and robust carbon dioxide electroreduction enabled by atomically dispersed Sn⁴⁺ sites. *Adv. Mater.* **2019**, *31*, 1808135.
- [97] Jiang, Z. L.; Wang, T.; Pei, J. J.; Shang, H. S.; Zhou, D. N.; Li, H. J.; Dong, J. C.; Wang, Y.; Cao, R.; Zhuang, Z. B. et al. Discovery of main group single Sb-N₄ active sites for CO₂ electroreduction to formate with high efficiency. *Energy Environ. Sci.* **2020**, *13*, 2856–2863.
- [98] Peterson, A. A.; Nørskov, J. K. Activity descriptors for CO₂ electroreduction to methane on transition-metal catalysts. *J. Phys. Chem. Lett.* **2012**, *3*, 251–258.
- [99] Kuhl, K. P.; Hatsukade, T.; Cave, E. R.; Abram, D. N.; Kibsgaard, J.; Jaramillo, T. F. Electrocatalytic conversion of carbon dioxide to methane and methanol on transition metal surfaces. *J. Am. Chem. Soc.* **2014**, *136*, 14107–14113.
- [100] Nie, X. W.; Esopi, M. R.; Janik, M. J.; Asthagiri, A. Selectivity of CO₂ reduction on copper electrodes: The role of the kinetics of elementary steps. *Angew. Chem., Int. Ed.* **2013**, *52*, 2459–2462.
- [101] Kuhl, K. P.; Cave, E. R.; Abram, D. N.; Jaramillo, T. F. New insights into the electrochemical reduction of carbon dioxide on metallic copper surfaces. *Energy Environ. Sci.* **2012**, *5*, 7050–7059.
- [102] Gao, D. F.; Arán-Ais, R. M.; Jeon, H. S.; Roldan Cuenya, B. Rational catalyst and electrolyte design for CO₂ electroreduction towards multicarbon products. *Nat. Catal.* **2019**, *2*, 198–210.
- [103] Monteiro, M. C. O.; Dattila, F.; Hagedorn, B.; García-Muelas, R.; López, N.; Koper, M. T. M. Absence of CO₂ electroreduction on copper, gold and silver electrodes without metal cations in solution. *Nat. Catal.* **2021**, *4*, 654–662.
- [104] Cai, Y. M.; Fu, J. J.; Zhou, Y.; Chang, Y. C.; Min, Q. H.; Zhu, J. J.; Lin, Y. H.; Zhu, W. L. Insights on forming N, O-coordinated Cu single-atom catalysts for electrochemical reduction CO₂ to methane. *Nat. Commun.* **2021**, *12*, 586.
- [105] Han, L. L.; Song, S. J.; Liu, M. J.; Yao, S. Y.; Liang, Z. X.; Cheng, H.; Ren, Z. H.; Liu, W.; Lin, R. Q.; Qi, G. C. et al. Stable and efficient single-atom Zn catalyst for CO₂ reduction to CH₄. *J. Am. Chem. Soc.* **2020**, *142*, 12563–12567.
- [106] Yang, H. P.; Wu, Y.; Li, G. D.; Lin, Q.; Hu, Q.; Zhang, Q. L.; Liu, J. H.; He, C. X. Scalable production of efficient single-atom copper decorated carbon membranes for CO₂ electroreduction to methanol. *J. Am. Chem. Soc.* **2019**, *141*, 12717–12723.
- [107] Guan, A. X.; Chen, Z.; Quan, Y. L.; Peng, C.; Wang, Z. Q.; Sham, T. K.; Yang, C.; Ji, Y. L.; Qian, L. P.; Xu, X. et al. Boosting CO₂ electroreduction to CH₄ via tuning neighboring single-copper sites. *ACS Energy Lett.* **2020**, *5*, 1044–1053.
- [108] Zhao, K.; Nie, X. W.; Wang, H. Z.; Chen, S.; Quan, X.; Yu, H. T.; Choi, W.; Zhang, G. H.; Kim, B.; Chen, J. G. Selective electroreduction of CO₂ to acetone by single copper atoms anchored on N-doped porous carbon. *Nat. Commun.* **2020**, *11*, 2455.
- [109] Karapinar, D.; Huan, N. T.; Ranjbar Sahraie, N.; Li, J. K.; Wakerley, D.; Touati, N.; Zanna, S.; Taverna, D.; Galvão Tizei, L. H.; Zitolo, A. et al. Electroreduction of CO₂ on single-site copper-nitrogen-doped carbon material: Selective formation of ethanol and reversible restructuration of the metal sites. *Angew. Chem., Int. Ed.* **2019**, *58*, 15098–15103.
- [110] Xu, H. P.; Rebollar, D.; He, H. Y.; Chong, L. N.; Liu, Y. Z.; Liu, C.; Sun, C. J.; Li, T.; Muntean, J. V.; Winans, R. E. et al. Highly selective electrocatalytic CO₂ reduction to ethanol by metallic clusters dynamically formed from atomically dispersed copper. *Nat. Energy* **2020**, *5*, 623–632.
- [111] Back, S.; Lim, J.; Kim, N. Y.; Kim, Y. H.; Jung, Y. Single-atom catalysts for CO₂ electroreduction with significant activity and selectivity improvements. *Chem. Sci.* **2017**, *8*, 1090–1096.
- [112] Huan, T. N.; Ranjbar, N.; Rousse, G.; Sougrati, M.; Zitolo, A.; Mougel, V.; Jaouen, F.; Fontecave, M. Electrochemical reduction of CO₂ catalyzed by Fe-N-C materials: A structure-selectivity study. *ACS Catal.* **2017**, *7*, 1520–1525.
- [113] Zhang, N. Q.; Zhang, X. X.; Tao, L.; Jiang, P.; Ye, C. L.; Lin, R.; Huang, Z. W.; Li, A.; Pang, D. W.; Yan, H. et al. Silver single-atom catalyst for efficient electrochemical CO₂ reduction synthesized from thermal transformation and surface reconstruction. *Angew. Chem., Int. Ed.* **2021**, *60*, 6170–6176.
- [114] Bagger, A.; Ju, W.; Varela, A. S.; Strasser, P.; Rossmeisl, J. Single site porphyrine-like structures advantages over metals for selective electrochemical CO₂ reduction. *Catal. Today* **2017**, *288*, 74–78.
- [115] Chen, W. X.; Pei, J. J.; He, C. T.; Wan, J. W.; Ren, H. L.; Zhu, Y. Q.; Wang, Y.; Dong, J. C.; Tian, S. B.; Cheong, W. C. et al. Rational design of single molybdenum atoms anchored on N-doped carbon for effective hydrogen evolution reaction. *Angew. Chem., Int. Ed.* **2017**, *56*, 16086–16090.
- [116] Chen, W. X.; Pei, J. J.; He, C. T.; Wan, J. W.; Ren, H. L.; Wang, Y.; Dong, J. C.; Wu, K. L.; Cheong, W. C.; Mao, J. J. et al. Single tungsten atoms supported on MOF-derived N-doped carbon for robust electrochemical hydrogen evolution. *Adv. Mater.* **2018**, *30*, 1800396.
- [117] Zhang, H. B.; Yu, L.; Chen, T.; Zhou, W.; Lou, X. W. Surface modulation of hierarchical MoS₂ nanosheets by Ni single atoms for enhanced electrocatalytic hydrogen evolution. *Adv. Funct. Mater.* **2018**, *28*, 1807086.
- [118] Shah, K.; Dai, R. Y.; Mateen, M.; Hassan, Z.; Zhuang, Z. W.; Liu, C. H.; Israr, M.; Cheong, W. C.; Hu, B. T.; Tu, R. Y. et al. Cobalt single atom incorporated in ruthenium oxide sphere: A robust bifunctional electrocatalyst for HER and OER. *Angew. Chem., Int. Ed.* **2022**, *61*, e202114951.
- [119] Varela, A. S.; Ju, W.; Bagger, A.; Franco, P.; Rossmeisl, J.; Strasser, P. Electrochemical reduction of CO₂ on metal-nitrogen-doped carbon catalysts. *ACS Catal.* **2019**, *9*, 7270–7284.
- [120] Li, X. G.; Bi, W. T.; Chen, M. L.; Sun, Y. X.; Ju, H. X.; Yan, W. S.; Zhu, J. F.; Wu, X. J.; Chu, W. S.; Wu, C. Z. et al. Exclusive Ni-N₄ sites realize near-unity CO selectivity for electrochemical CO₂ reduction. *J. Am. Chem. Soc.* **2017**, *139*, 14889–14892.
- [121] Han, N.; Wang, Y.; Ma, L.; Wen, J. G.; Li, J.; Zheng, H. C.; Nie, K. Q.; Wang, X. X.; Zhao, F. P.; Li, Y. G. et al. Supported cobalt polyphthalocyanine for high-performance electrocatalytic CO₂ reduction. *Chem* **2017**, *3*, 652–664.
- [122] Lin, L.; Li, H. B.; Wang, Y.; Li, H. F.; Wei, P. F.; Nan, B.; Si, R.; Wang, G. X.; Bao, X. H. Temperature-dependent CO₂ electroreduction over Fe-N-C and Ni-N-C single-atom catalysts. *Angew. Chem., Int. Ed.* **2021**, *60*, 26582–26586.
- [123] Wang, Y.; You, L. M.; Zhou, K. Origin of the N-coordinated single-atom Ni sites in heterogeneous electrocatalysts for CO₂ reduction reaction. *Chem. Sci.* **2021**, *12*, 14065–14073.
- [124] Gu, J.; Hsu, C. S.; Bai, L. C.; Chen, H. M.; Hu, X. L. Atomically dispersed Fe³⁺ sites catalyze efficient CO₂ electroreduction to CO. *Science* **2019**, *364*, 1091–1094.
- [125] Wang, X. Q.; Chen, Z.; Zhao, X. Y.; Yao, T.; Chen, W. X.; You, R.; Zhao, C. M.; Wu, G.; Wang, J.; Huang, W. X. et al. Regulation of coordination number over single Co sites: Triggering the efficient electroreduction of CO₂. *Angew. Chem., Int. Ed.* **2018**, *57*, 1944–1948.
- [126] Rong, X.; Wang, H. J.; Lu, X. L.; Si, R.; Lu, T. B. Controlled synthesis of a vacancy-defect single-atom catalyst for boosting CO₂ electroreduction. *Angew. Chem., Int. Ed.* **2020**, *59*, 1961–1965.
- [127] Yan, C. C.; Li, H. B.; Ye, Y. F.; Wu, H. H.; Cai, F.; Si, R.; Xiao, J. P.; Miao, S.; Xie, S. H.; Yang, F. et al. Coordinatively unsaturated

- nickel-nitrogen sites towards selective and high-rate CO₂ electroreduction. *Energy Environ. Sci.* **2018**, *11*, 1204–1210.
- [128] Yang, H. B.; Hung, S. F.; Liu, S.; Yuan, K. D.; Miao, S.; Zhang, L. P.; Huang, X.; Wang, H. Y.; Cai, W. Z.; Chen, R. et al. Atomically dispersed Ni(I) as the active site for electrochemical CO₂ reduction. *Nat. Energy* **2018**, *3*, 140–147.
- [129] Kim, H.; Shin, D.; Yang, W.; Won, D. H.; Oh, H. S.; Chung, M. W.; Jeong, D.; Kim, S. H.; Chae, K. H.; Ryu, J. Y. et al. Identification of single-atom Ni site active toward electrochemical CO₂ conversion to CO. *J. Am. Chem. Soc.* **2021**, *143*, 925–933.
- [130] Hossain, D.; Huang, Y. F.; Yu, T. H.; Goddard III, W. A.; Luo, Z. T. Reaction mechanism and kinetics for CO₂ reduction on nickel single atom catalysts from quantum mechanics. *Nat. Commun.* **2020**, *11*, 2256.
- [131] Kramer, W. W.; McCrory, C. C. L. Polymer coordination promotes selective CO₂ reduction by cobalt phthalocyanine. *Chem. Sci.* **2016**, *7*, 2506–2515.
- [132] Pan, Y.; Lin, R.; Chen, Y. J.; Liu, S. J.; Zhu, W.; Cao, X.; Chen, W. X.; Wu, K. L.; Cheong, W. C.; Wang, Y. et al. Design of single-atom Co-N₅ catalytic site: A robust electrocatalyst for CO₂ reduction with nearly 100% CO selectivity and remarkable stability. *J. Am. Chem. Soc.* **2018**, *140*, 4218–4221.
- [133] Zhang, B. X.; Zhang, J. L.; Shi, J. B.; Tan, D. X.; Liu, L. F.; Zhang, F. Y.; Lu, C.; Su, Z. Z.; Tan, X. N.; Cheng, X. Y. et al. Manganese acting as a high-performance heterogeneous electrocatalyst in carbon dioxide reduction. *Nat. Commun.* **2019**, *10*, 2980.
- [134] Zee, D. Z.; Nippe, M.; King, A. E.; Chang, C. J.; Long, J. R. Tuning second coordination sphere interactions in polypyridyl-iron complexes to achieve selective electrocatalytic reduction of carbon dioxide to carbon monoxide. *Inorg. Chem.* **2020**, *59*, 5206–5217.
- [135] Nichols, A. W.; Hooe, S. L.; Kuehner, J. S.; Dickie, D. A.; Machan, C. W. Electrocatalytic CO₂ reduction to formate with molecular Fe(III) complexes containing pendent proton relays. *Inorg. Chem.* **2020**, *59*, 5854–5864.
- [136] Azcarate, I.; Costentin, C.; Robert, M.; Savéant, J. M. Through-space charge interaction substituent effects in molecular catalysis leading to the design of the most efficient catalyst of CO₂-to-CO electrochemical conversion. *J. Am. Chem. Soc.* **2016**, *138*, 16639–16644.
- [137] Tang, J. K.; Zhu, C. Y.; Jiang, T. W.; Wei, L.; Wang, H.; Yu, K.; Yang, C. L.; Zhang, Y. B.; Chen, C.; Li, Z. T. et al. Anion exchange-induced single-molecule dispersion of cobalt porphyrins in a cationic porous organic polymer for enhanced electrochemical CO₂ reduction via secondary-coordination sphere interactions. *J. Mater. Chem. A* **2020**, *8*, 18677–18686.
- [138] Weng, Z.; Jiang, J. B.; Wu, Y. S.; Wu, Z. S.; Guo, X. T.; Materna, K. L.; Liu, W.; Batista, V. S.; Brudvig, G. W.; Wang, H. L. Electrochemical CO₂ reduction to hydrocarbons on a heterogeneous molecular Cu catalyst in aqueous solution. *J. Am. Chem. Soc.* **2016**, *138*, 8076–8079.
- [139] Wu, Y. S.; Jiang, Z.; Lu, X.; Liang, Y. Y.; Wang, H. L. Domino electroreduction of CO₂ to methanol on a molecular catalyst. *Nature* **2019**, *575*, 639–642.
- [140] Chen, S. H.; Li, W. H.; Jiang, W. J.; Yang, J. R.; Zhu, J. X.; Wang, L. Q.; Ou, H. H.; Zhuang, Z. C.; Chen, M. Z.; Sun, X. H. et al. MOF encapsulating N-heterocyclic carbene-ligated copper single-atom site catalyst towards efficient methane electrosynthesis. *Angew. Chem., Int. Ed.* **2022**, *61*, e202114450.
- [141] Sun, X. H.; Tuo, Y. X.; Ye, C. L.; Chen, C.; Lu, Q.; Li, G. N.; Jiang, P.; Chen, S. H.; Zhu, P.; Ma, M. et al. Phosphorus induced electron localization of single iron sites for boosted CO₂ electroreduction reaction. *Angew. Chem., Int. Ed.* **2021**, *60*, 23614–23618.
- [142] Zhang, X.; Wu, Z. S.; Zhang, X.; Li, L. W.; Li, Y. Y.; Xu, H. M.; Li, X. X.; Yu, X. L.; Zhang, Z. S.; Liang, Y. Y. et al. Highly selective and active CO₂ reduction electrocatalysts based on cobalt phthalocyanine/carbon nanotube hybrid structures. *Nat. Commun.* **2017**, *8*, 14675.
- [143] Liang, F. X.; Zhang, J.; Hu, Z. W.; Ma, C.; Ni, W. P.; Zhang, Y.; Zhang, S. G. Intrinsic defect-rich graphene coupled cobalt phthalocyanine for robust electrochemical reduction of carbon dioxide. *ACS Appl. Mater. Interfaces* **2021**, *13*, 25523–25532.
- [144] Zhang, C.; Li, Y. L. Graphdiyne based atomic catalyst: An emerging star for energy conversion. *Chem. Res. Chin. Univ.* **2021**, *37*, 1149–1157.
- [145] Liu, X.; Wang, Z. X.; Tian, Y.; Zhao, J. X. Graphdiyne-supported single iron atom: A promising electrocatalyst for carbon dioxide electroreduction into methane and ethanol. *J. Phys. Chem. C* **2020**, *124*, 3722–3730.
- [146] Gu, H. L.; Zhong, L. X.; Shi, G. S.; Li, J. Q.; Yu, K.; Li, J.; Zhang, S.; Zhu, C. Y.; Chen, S. H.; Yang, C. L. et al. Graphdiyne/graphene heterostructure: A universal 2D scaffold anchoring monodispersed transition-metal phthalocyanines for selective and durable CO₂ electroreduction. *J. Am. Chem. Soc.* **2021**, *143*, 8679–8688.
- [147] Wang, J.; Huang, X.; Xi, S. B.; Xu, H.; Wang, X. Axial modification of cobalt complexes on heterogeneous surface with enhanced electron transfer for carbon dioxide reduction. *Angew. Chem., Int. Ed.* **2020**, *59*, 19162–19167.
- [148] Huang, N.; Lee, K. H.; Yue, Y.; Xu, X. Y.; Irle, S.; Jiang, Q. H.; Jiang, D. L. A stable and conductive metallophthalocyanine framework for electrocatalytic carbon dioxide reduction in water. *Angew. Chem., Int. Ed.* **2020**, *59*, 16587–16593.
- [149] Zhong, H. X.; Ghorbani-Asl, M.; Ly, K. H.; Zhang, J. C.; Ge, J.; Wang, M. C.; Liao, Z. Q.; Makarov, D.; Zschech, E.; Brunner, E. et al. Synergistic electroreduction of carbon dioxide to carbon monoxide on bimetallic layered conjugated metal-organic frameworks. *Nat. Commun.* **2020**, *11*, 1409.
- [150] Wen, C. F.; Mao, F. X.; Liu, Y. W.; Zhang, X. Y.; Fu, H. Q.; Zheng, L. R.; Liu, P. F.; Yang, H. G. Nitrogen-stabilized low-valent Ni motifs for efficient CO₂ electrocatalysis. *ACS Catal.* **2020**, *10*, 1086–1093.
- [151] Lin, L.; Liu, T. F.; Xiao, J. P.; Li, H. F.; Wei, P. F.; Gao, D. F.; Nan, B.; Si, R.; Wang, G. X.; Bao, X. H. Enhancing CO₂ electroreduction to methane with a cobalt phthalocyanine and zinc-nitrogen-carbon tandem catalyst. *Angew. Chem., Int. Ed.* **2020**, *59*, 22408–22413.
- [152] Lin, L.; Li, H. B.; Yan, C. C.; Li, H. F.; Si, R.; Li, M. R.; Xiao, J. P.; Wang, G. X.; Bao, X. H. Synergistic catalysis over iron-nitrogen sites anchored with cobalt phthalocyanine for efficient CO₂ electroreduction. *Adv. Mater.* **2019**, *31*, 1903470.
- [153] Meng, D. L.; Zhang, M. D.; Si, D. H.; Mao, M. J.; Hou, Y.; Huang, Y. B.; Cao, R. Highly selective tandem electroreduction of CO₂ to ethylene over atomically isolated nickel-nitrogen site/copper nanoparticle catalysts. *Angew. Chem., Int. Ed.* **2021**, *60*, 25485–25492.
- [154] Li, F. W.; Li, Y. C.; Wang, Z. Y.; Li, J.; Nam, D. H.; Lum, Y. W.; Luo, M. C.; Wang, X.; Ozden, A.; Hung, S. F. et al. Cooperative CO₂-to-ethanol conversion via enriched intermediates at molecule-metal catalyst interfaces. *Nat. Catal.* **2020**, *3*, 75–82.
- [155] Zhang, N. Q.; Zhang, X. X.; Kang, Y. K.; Ye, C. L.; Jin, R.; Yan, H.; Lin, R.; Yang, J. R.; Xu, Q.; Wang, Y. et al. A supported Pd₂ dual-atom site catalyst for efficient electrochemical CO₂ reduction. *Angew. Chem., Int. Ed.* **2021**, *60*, 13388–13393.
- [156] Zhang, H. C.; Chang, X. X.; Chen, J. G.; Goddard III, W. A.; Xu, B. J.; Cheng, M. J.; Lu, Q. Computational and experimental demonstrations of one-pot tandem catalysis for electrochemical carbon dioxide reduction to methane. *Nat. Commun.* **2019**, *10*, 3340.
- [157] Ren, D.; Ang, B. S. H.; Yeo, B. S. Tuning the selectivity of carbon dioxide electroreduction toward ethanol on oxide-derived Cu_xZn catalysts. *ACS Catal.* **2016**, *6*, 8239–8247.
- [158] Morales-Guio, C. G.; Cave, E. R.; Nitopi, S. A.; Feaster, J. T.; Wang, L.; Kuhl, K. P.; Jackson, A.; Johnson, N. C.; Abram, D. N.; Hatsukade, T. et al. Improved CO₂ reduction activity towards C₂₊ alcohols on a tandem gold on copper electrocatalyst. *Nat. Catal.* **2018**, *1*, 764–771.
- [159] Jouny, M.; Luc, W.; Jiao, F. High-rate electroreduction of carbon monoxide to multi-carbon products. *Nat. Catal.* **2018**, *1*, 748–755.

- [160] Hou, Y.; Huang, Y. B.; Liang, Y. L.; Chai, G. L.; Yi, J. D.; Zhang, T.; Zang, K. T.; Luo, J.; Xu, R.; Lin, H. et al. Unraveling the reactivity and selectivity of atomically isolated metal–nitrogen sites anchored on porphyrinic triazine frameworks for electroreduction of CO₂. *CCS Chem.* **2019**, *1*, 384–395.
- [161] Gao, D. F.; Liu, T. F.; Wang, G. X.; Bao, X. H. Structure sensitivity in single-atom catalysis toward CO₂ electroreduction. *ACS Energy Lett.* **2021**, *6*, 713–727.
- [162] Zou, Y. Q.; Wang, S. Y. An investigation of active sites for electrochemical CO₂ reduction reactions: From *in situ* characterization to rational design. *Adv. Sci.* **2021**, *8*, 2003579.
- [163] Nguyen, T. N.; Dinh, C. T. Gas diffusion electrode design for electrochemical carbon dioxide reduction. *Chem. Soc. Rev.* **2020**, *49*, 7488–7504.
- [164] García de Arquer, F. P.; Dinh, C. T.; Ozden, A.; Wicks, J.; McCallum, C.; Kirmani, A. R.; Nam, D. H.; Gabardo, C.; Seifitokaldani, A.; Wang, X. et al. CO₂ electrolysis to multicarbon products at activities greater than 1 A·cm⁻². *Science* **2020**, *367*, 661–666.
- [165] Ma, W. C.; Xie, S. J.; Liu, T. T.; Fan, Q. Y.; Ye, J. Y.; Sun, F. F.; Jiang, Z.; Zhang, Q. H.; Cheng, J.; Wang, Y. Electrocatalytic reduction of CO₂ to ethylene and ethanol through hydrogen-assisted C–C coupling over fluorine-modified copper. *Nat. Catal.* **2020**, *3*, 478–487.